

Correlation functions in liquids and crystals : Free energy functional and liquid - crystal transition

Atul S. Bharadwaj, Swarn L. Singh* and Yashwant Singh

Department of Physics, Banaras Hindu University, Varanasi-221 005, India.

(Dated: April 4, 2013)

Abstract

A free energy functional for a crystal that contains both the symmetry conserved and symmetry broken parts of the direct pair correlation function has been used to investigate the crystallization of fluids in three-dimensions. The symmetry broken part of the direct pair correlation function has been calculated using a series in ascending powers of the order parameters and which contains three- and higher-bodies direct correlation functions of the isotropic phase. It is shown that a very accurate description of freezing transitions for a wide class of potentials is found by considering the first two terms of this series. The results found for freezing parameters including structure of the frozen phase for fluids interacting via the inverse power potential $u(r) = \epsilon (\sigma/r)^n$ for n ranging from 4 to ∞ are in very good agreement with simulation results. It is found that for $n > 6.5$ the fluid freezes into a face centred cubic (fcc) structure while for $n \leq 6$ the body centred cubic (bcc) structure is preferred. The fluid-bcc-fcc triple point is found to be at $1/n = 0.158$ which is in good agreement with simulation result.

PACS numbers: 64.70.D-, 05.70.Fh, 64.70.pm

[1] * Present address-Max Planck Institute for Intelligent Systems, Heisenbergstr. 3, 70569 Stuttgart, Germany, and Institut für Theoretische Physik IV, Universität Stuttgart, Pfaffenwaldring 57, 70569 Stuttgart, Germany.

I. INTRODUCTION

Freezing of a fluid into a crystalline solid is a particular, but an important example of a first-order phase transition in which the continuous symmetry of the fluid is broken into one of the Bravais lattices. The transition in three-dimensions is marked by large discontinuities in entropy, density and order parameters; the order parameters being proportional to the lattice components of one particle density distribution $\rho(\vec{r})$ (see Eq.(2.3)). Efforts have been made for over six decades [1, 2] to find a first principle theory which can answer questions such as, at what density, pressure and temperature does a particular liquid freeze ? What is the change in entropy and the change in density upon freezing ? Which of the Bravais lattices emerges at the freezing point for a given system and what are values of the order parameters?

A crystal is a system of extreme inhomogeneities where value of $\rho(\vec{r})$ shows several orders of magnitude difference between its values on the lattice sites and in the interstitial regions. The density functional formalism of classical statistical mechanics has been employed to develop theories for freezing transitions [2, 3]. This kind of approach was initiated in 1979 by Ramakrishnan and Yussouff (RY) [4] which was latter reformulated by Haymet and Oxtoby [5]. The central quantity in this formalism is the reduced Helmholtz free energy of both the crystal, $A[\rho]$, and the liquid, $A(\rho_l)$ [2]. For crystals, $A[\rho]$ is a unique functional of $\rho(\vec{r})$ whereas for liquids, $A(\rho_l)$ is simply a function of liquid density ρ_l which is a constant, independent of position.

The density functional formalism is used to write an expression for $A[\rho]$ (or for the grand thermodynamic potential) in terms of $\rho(\vec{r})$ and the direct pair correlation function (DPCF). Minimization of this expression with respect to $\rho(\vec{r})$ leads to an expression that relates $\rho(\vec{r})$ to the DPCF. The DPCF that appears in these equations corresponds to the crystal and is functional of $\rho(\vec{r})$ and therefore depends on values of the order parameters. In the RY theory the functional dependence of the DPCF on $\rho(\vec{r})$ was neglected and was replaced by that of the coexisting liquid of density ρ_l . Attempts to improve the RY theory by incorporating a term involving three-body direct correlation function of the coexisting liquid in the expression of $A[\rho]$ have failed [6, 7]. The efforts made by Tarazona [8], Curtin, Ashcraft and Denton [9, 10] and others [11, 12] in the direction of developing a theory using what is referred to as the *weighted density approximation* have also met with limited success

only.

The reason, as has been pointed out recently [13, 14], is that at the fluid - solid transition the isotropy and the homogeneity of space is spontaneously broken and a qualitatively new contribution to the correlation in distribution of particles emerges. This fact has been used to write the DPCF of the frozen phase as a sum of two terms; one that preserves the continuous symmetry of the liquid and the other that breaks it and vanishes in the liquid. An exact expression for the free energy functional was found by performing double functional integration in density space of a relation that relates the second functional derivative of $A[\rho]$ with respect to $\rho(\vec{r})$ to the DPCF (see Eq.(2.7)). This expression of free energy functional contains both the symmetry conserved and the symmetry broken parts of the DPCF.

The values of the DPCF as well as of the total pair correlation function (described in Sec II) in a classical system can be found from solution of integral equation, the Ornstein - Zernike (OZ) equation, and a closure relation that relates correlation functions to pair potential [15]. The integral equation theory has been quite successful in getting values of pair correlation functions of uniform liquids [15], but its application to find pair correlation functions of symmetry broken phases has so far been limited. Recently Mishra and Singh [16] have used the OZ equation and the Percus - Yevick (PY) closure relation to obtain both the symmetry conserved and symmetry broken parts of pair correlation functions in a nematic phase. In the nematic phase the orientational symmetry is broken but the translational symmetry of the liquid phase remains intact whereas in a crystal both the orientational and the translational symmetries of the liquid phase are broken. Since, closure relations are derived assuming translational invariance [15], they are valid in normal liquids as well as in nematics but may not in crystals. In view of this, Singh and Singh [13] suggested a method in which the symmetry broken part of the DPCF is expanded in ascending powers of order parameters. This series contains three- and higher - bodies direct correlation functions of the isotropic phase. The first term of this series was evaluated and used in investigating the freezing transitions in two- and three-dimensions of fluids interacting via inverse power potentials [13, 17] and freezing of hard spheres into crystalline and glassy phases [14]. It has been found that contribution made by the symmetry broken part to the grand thermodynamic potential at the freezing point increases with softness of the potential [13, 17]. This suggests that for long - ranged potentials the higher order terms of the series may not be negligible and need to be considered.

In this paper we calculate first and second terms of the series (see Eq.(2.29)) which involve three and four-bodies direct correlation functions of the isotropic phase. We calculate the four-body direct correlation function by extending the method developed to calculate the three-body direct correlation function. The values found for the DPCF are used in the free-energy functional and the crystallization of fluids is investigated. We show that all questions posed at the beginning of this section are correctly answered for a wide class of potentials.

The paper is organised as follows: In Sec. II we describe correlation functions in liquids and in crystals and calculate them. The symmetry broken part of the DPCF is evaluated using first two terms of a series in ascending powers of order parameters. These results are used in the free-energy functional in Sec. III to calculate the contributions made by different parts of the DPCF to the grand thermodynamic potential at the freezing point. In Sec. IV we calculate these terms and locate the freezing points for fluids interacting via the inverse power potentials and compare our results with those found from computer simulations and from approximate free energy functionals. The paper ends with a brief summary and perspectives given in Sec. V.

II. CORRELATION FUNCTIONS

The equilibrium one particle distribution $\rho(\vec{r})$ defined as

$$\rho(\vec{r}) = \left\langle \sum_l \delta(\vec{r} - \vec{r}_l) \right\rangle, \quad (2.1)$$

where \vec{r}_l is position vector of the l^{th} particle and the angular bracket, $\langle \dots \rangle$, represents the ensemble average, is a constant, independent of position for a normal liquid but contains most of the structural informations of a crystal. For a crystalline solid there exists a discrete set of vectors \vec{R}_i such that,

$$\rho(\vec{r}) = \rho(\vec{r} + \vec{R}_i), \quad \text{for all } \vec{R}_i. \quad (2.2)$$

This set of vectors which appears at the freezing point due to spontaneous breaking of continuous symmetry of a liquid, necessarily forms a Bravais lattice. The $\rho(\vec{r})$ in a crystal

can be written as a sum of two terms:

$$\rho(\vec{r}) = \rho_0 + \rho^{(b)}(\vec{r}) \quad (2.3a)$$

where

$$\rho^{(b)}(\vec{r}) = \sum_G \rho_G e^{i\vec{G}\cdot\vec{r}}. \quad (2.3b)$$

Here ρ_0 is the average density of the crystal and ρ_G are the order parameters (amplitude of density waves of wavelength $2\pi/|\vec{G}|$). The sum in Eq.(2.3b) is over a complete set of reciprocal lattice vectors (RLV) \vec{G} with the property that $e^{i\vec{G}\cdot\vec{R}_i} = 1$ for all \vec{G} and for all \vec{R}_i . We refer the first term of Eq.(2.3a) as symmetry conserved and the second as symmetry broken parts of single particle distribution $\rho(\vec{r})$.

The two-particle density distribution $\rho^{(2)}(\vec{r}_1, \vec{r}_2)$ which gives probability of finding simultaneously a particle in volume element $d\vec{r}_1$ at \vec{r}_1 and a second particle in volume element $d\vec{r}_2$ at \vec{r}_2 , is defined as

$$\rho^{(2)}(\vec{r}_1, \vec{r}_2) = \left\langle \sum_j \sum_{k \neq j} \delta(\vec{r}_1 - \vec{r}_j) \delta(\vec{r}_2 - \vec{r}_k) \right\rangle. \quad (2.4)$$

The pair correlation function $g(\vec{r}_1, \vec{r}_2)$ is related to $\rho^{(2)}(\vec{r}_1, \vec{r}_2)$ by the relation,

$$g(\vec{r}_1, \vec{r}_2) = \frac{\rho^{(2)}(\vec{r}_1, \vec{r}_2)}{\rho(\vec{r}_1)\rho(\vec{r}_2)}. \quad (2.5)$$

The DPCF $c(\vec{r}_1, \vec{r}_2)$, which appears in the expression of free-energy functional $A[\rho]$ is related to the total pair correlation function $h(\vec{r}_1, \vec{r}_2) = g(\vec{r}_1, \vec{r}_2) - 1$ through the Ornstein - Zernike (OZ) equation [2]

$$c(\vec{r}_1, \vec{r}_2) = h(\vec{r}_1, \vec{r}_2) - \int d\vec{r}_3 c(\vec{r}_1, \vec{r}_3) \rho(\vec{r}_3) h(\vec{r}_2, \vec{r}_3). \quad (2.6)$$

The second functional derivative of $A[\rho]$ is expressed in terms of $c(\vec{r}_1, \vec{r}_2)$ as [2]

$$\frac{\delta^2 A[\rho]}{\delta\rho(\vec{r}_1) \delta\rho(\vec{r}_2)} = \frac{\delta(\vec{r}_1 - \vec{r}_2)}{\rho(\vec{r}_1)} - c(\vec{r}_1, \vec{r}_2), \quad (2.7)$$

where δ is Dirac function. The first term on the right hand side of this equation corresponds to ideal part $A_{id}[\rho]$ of the free energy whereas the second term corresponds to excess part $A_{ex}[\rho]$ arising due to interparticle interactions.

In a normal liquid all pair correlation functions defined above are simple function of number density ρ and depend only on magnitude of interparticle separation $|\vec{r}_2 - \vec{r}_1| = r$. This simplification is due to homogeneity which implies continuous translational symmetry and isotropy which implies continuous rotational symmetry. In a crystal which is both inhomogeneous and anisotropic, pair correlation functions can be written as a sum of two terms; one that preserves the continuous symmetry of the liquid and the other that breaks it [13, 16]. Thus

$$h(\vec{r}_1, \vec{r}_2) = h^{(0)}(|\vec{r}_2 - \vec{r}_1|, \rho_0) + h^{(b)}(\vec{r}_1, \vec{r}_2; [\rho]) \quad (2.8)$$

$$c(\vec{r}_1, \vec{r}_2) = c^{(0)}(|\vec{r}_2 - \vec{r}_1|, \rho_0) + c^{(b)}(\vec{r}_1, \vec{r}_2; [\rho]). \quad (2.9)$$

While the symmetry conserving part ($h^{(0)}$ and $c^{(0)}$) depends on the magnitude of interparticle separation r and is a function of average density ρ_0 , the symmetry broken parts $h^{(b)}$ and $c^{(b)}$ are functional of $\rho(\vec{r})$ (indicated by square bracket) and are invariant only under a discrete set of translations corresponding to lattice vectors \vec{R}_i ,

$$h^{(b)}(\vec{r}_1, \vec{r}_2) = h^{(b)}(\vec{r}_1 + \vec{R}_i, \vec{r}_2 + \vec{R}_i) \quad (2.10)$$

$$c^{(b)}(\vec{r}_1, \vec{r}_2) = c^{(b)}(\vec{r}_1 + \vec{R}_i, \vec{r}_2 + \vec{R}_i) \quad (2.11)$$

If one chooses a centre of mass variable $\vec{r}_c = (\vec{r}_1 + \vec{r}_2)/2$ and a difference variable $\vec{r} = \vec{r}_2 - \vec{r}_1$, then one can see from Eqs. (2.10) and (2.11) that $h^{(b)}$ and $c^{(b)}$ are periodic functions of the centre of mass variable and a continuous function of the difference variable [18]. Thus

$$h^{(b)}(\vec{r}_1, \vec{r}_2) = \sum_G e^{i\vec{G} \cdot \vec{r}_c} h^{(G)}(\vec{r}) \quad (2.12)$$

$$c^{(b)}(\vec{r}_1, \vec{r}_2) = \sum_G e^{i\vec{G} \cdot \vec{r}_c} c^{(G)}(\vec{r}) \quad (2.13)$$

Since $h^{(G)}$ and $c^{(G)}$ are real and symmetric with respect to interchange of \vec{r}_1 and \vec{r}_2 ; $h^{(-G)}(\vec{r}) = h^{(G)}(\vec{r})$ and $h^{(G)}(-\vec{r}) = h^{(G)}(\vec{r})$ and similar relations holds for $c^{(G)}(\vec{r})$.

Substitution of values of $h(\vec{r}_1, \vec{r}_2)$ and $c(\vec{r}_1, \vec{r}_2)$ given by Eqs. (2.8) and (2.9) in Eq. (2.6) allows us to split the OZ equation into two equations; one that contains $h^{(0)}$, $c^{(0)}$ and ρ_0 while the other contains $h^{(b)}$, $c^{(b)}$ and $\rho(\vec{r}_3)$ along with $h^{(0)}$, $c^{(0)}$ and ρ_0 :

$$h^{(0)}(|\vec{r}_2 - \vec{r}_1|) = c^{(0)}(|\vec{r}_2 - \vec{r}_1|) + \rho_0 \int d\vec{r}_3 c^{(0)}(|\vec{r}_3 - \vec{r}_1|) h^{(0)}(|\vec{r}_3 - \vec{r}_2|) \quad (2.14)$$

and

$$\begin{aligned} h^{(b)}(\vec{r}_1, \vec{r}_2) &= c^{(b)}(\vec{r}_1, \vec{r}_2) + \int d\vec{r}_3 c^{(0)}(|\vec{r}_3 - \vec{r}_1|) (\rho(\vec{r}_3) - \rho_0) h^{(0)}(|\vec{r}_3 - \vec{r}_2|) \\ &+ \int d\vec{r}_3 \rho(\vec{r}_3) [c^{(b)}(\vec{r}_1, \vec{r}_3) h^{(0)}(|\vec{r}_3 - \vec{r}_2|) + c^{(0)}(|\vec{r}_3 - \vec{r}_2|) h^{(b)}(\vec{r}_1, \vec{r}_3) \\ &+ c^{(b)}(\vec{r}_1, \vec{r}_3) h^{(b)}(\vec{r}_1, \vec{r}_3)]. \end{aligned} \quad (2.15)$$

Eq. (2.14) is the well known OZ equation of normal liquids. We use it along with a closure relation to calculate the values of these correlation functions and their derivatives with respect to density ρ_0 . The derivatives of $c^{(0)}(r)$ are used to find values of three- and four- bodies direct correlation functions of the isotropic phase.

Eq. (2.15) is the OZ equation for symmetry broken part of correlation functions. In order to make use of it to find values of $h^{(b)}$ and $c^{(b)}$ for a given $\rho(\vec{r})$ we need one more relation (closure relation) that connects $h^{(b)}$ with $c^{(b)}$. Alternatively, if we know values of one of these functions then Eq. (2.15) can be used to find values of the other function [19]. Here we calculate $c^{(b)}(\vec{r}_1, \vec{r}_2)$ using a series in ascending powers of $(\rho(\vec{r}) - \rho_0)$.

A. Calculation of $h^{(0)}$, $c^{(0)}$ and their derivatives with respect to ρ

We use the OZ equation (2.14) and a closure relation proposed by Roger and Young [20] which mixes the Percus-Yevick (PY) relation and the hypernetted chain (HNC) relation in such a way that at $r = 0$ it reduces to the PY relation and for $r \rightarrow \infty$ it reduces to the HNC relation and is written as

$$h^{(0)}(r) = \exp[-\beta u(r)] \left[1 + \frac{\exp[\chi(r)f(r)]}{f(r)} \right] - 1 \quad (2.16)$$

where $\chi(r) = h^{(0)}(r) - c^{(0)}(r)$ and $f(r) = 1 - \exp(-\psi r)$ is a mixing function with adjustable parameter $0 \leq \psi \leq \infty$, to calculate pair correlation functions and their derivatives with respect to density ρ . The value of ψ is chosen to guarantee thermodynamic consistency between the virial and compressibility routes to the equation of state [20].

The differentiation of Eqs. (2.14) and (2.16) with respect to ρ yields the following relations,

$$\begin{aligned}\frac{\partial h^{(0)}(r)}{\partial \rho} &= \frac{\partial c^{(0)}(r)}{\partial \rho} + \int d\vec{r}' c^{(0)}(r') h^{(0)}(|\vec{r}' - \vec{r}|) \\ &\quad + \rho \int d\vec{r}' \frac{\partial c^{(0)}(r')}{\partial \rho} h^{(0)}(|\vec{r}' - \vec{r}|) \\ &\quad + \rho \int d\vec{r}' c^{(0)}(r') \frac{\partial h^{(0)}(|\vec{r}' - \vec{r}|)}{\partial \rho}\end{aligned}\quad (2.17)$$

and

$$\frac{\partial h^{(0)}(r)}{\partial \rho} = \exp[-\beta u(r)] \exp[\chi(r) f(r)] \frac{\partial \chi(r)}{\partial \rho}, \quad (2.18)$$

$$\begin{aligned}\frac{\partial^2 h^{(0)}(r)}{\partial \rho^2} &= \frac{\partial^2 c^{(0)}(r)}{\partial \rho^2} + 2 \int d\vec{r}' \left[\frac{\partial c^{(0)}(r')}{\partial \rho} h^{(0)}(|\vec{r}' - \vec{r}|) + c^{(0)}(r') \frac{\partial h^{(0)}(|\vec{r}' - \vec{r}|)}{\partial \rho} \right] \\ &\quad + \rho \int d\vec{r}' \left[2 \frac{\partial c^{(0)}(r')}{\partial \rho} \frac{\partial h^{(0)}(|\vec{r}' - \vec{r}|)}{\partial \rho} + c^{(0)}(r') \frac{\partial^2 h^{(0)}(|\vec{r}' - \vec{r}|)}{\partial \rho^2} \right. \\ &\quad \left. + \frac{\partial^2 c^{(0)}(r')}{\partial \rho^2} h^{(0)}(|\vec{r}' - \vec{r}|) \right]\end{aligned}\quad (2.19)$$

and

$$\frac{\partial^2 h^{(0)}(r)}{\partial \rho^2} = \exp[-\beta u(r)] \exp[\chi(r) f(r)] \left[\frac{\partial^2 \chi(r)}{\partial \rho^2} + \left(\frac{\partial \chi(r)}{\partial \rho} \right)^2 f(r) \right]. \quad (2.20)$$

The solution of the closed set of coupled equations (2.14) and (2.17)-(2.20) gives values of $h^{(0)}(r)$, $c^{(0)}(r)$, $\frac{\partial h^{(0)}(r)}{\partial \rho}$, $\frac{\partial c^{(0)}(r)}{\partial \rho}$, $\frac{\partial^2 h^{(0)}(r)}{\partial \rho^2}$ and $\frac{\partial^2 c^{(0)}(r)}{\partial \rho^2}$ as a function of r for a given potential $u(r)$.

The pair potential taken here are the inverse power potentials, $u(r) = \epsilon(\sigma/r)^n$ where ϵ , σ and n are potential parameters and r is the molecular separation. The parameter n measures softness of the potential; $n = \infty$ corresponds to hard-sphere and $n = 1$ to the one component plasma. The reason for our choosing these potentials is that the range of potential can be varied by changing the value of n and the fact that the equation of state and melting curves of these potentials have been extensively investigated by computer simulations [21–28] for several values of n so that "exact" results are available for comparison. The more repulsive

($n \geq 7$) systems have been found to freeze into a face-centred cubic (fcc) structure while the soft repulsions $n < 7$ freeze into a body-centred cubic crystal (bcc) structure. The fluid-bcc-fcc triple point is found to occur at $\frac{1}{n} \simeq 0.15$ [25, 26, 28]. The atomic arrangements in the two cubic structures are very different; the fcc is close-packed in real space and the density inhomogeneity is much sharper than for the bcc which is open structure in real space but close-packed in Fourier space. However, in spite of this difference in the atomic arrangements, the two structures have small difference in free energy (or chemical potential) at the fluid - solid transition [25–28] and therefore a correct description of the relative stability of the two cubic structures is a stringent test for any theory.

The inverse power potentials are known to have a simple scaling property according to which the reduced thermodynamic properties depend on a single variable which is defined as

$$\gamma = \rho\sigma^3 (\beta\epsilon)^{3/n} = \rho^* T^{*(-3/n)}$$

where $\beta = 1/k_B T$; k_B is the Boltzmann constant and T temperature. Using the scaling relation the potential is written as

$$\beta u(r) = \left(\frac{4\pi}{3} \gamma \right)^{n/3} \frac{1}{r^n}$$

where r is measured in unit of $a_0 = \left(\frac{3}{4\pi\rho} \right)^{1/3}$.

In Fig. 1 we plot values of $c^{(0)}(r)$, $\frac{\partial c^{(0)}(r)}{\partial \rho}$ and $\frac{\partial^2 c^{(0)}(r)}{\partial \rho^2}$ for $n = 6$ and $\gamma = 2.30$ which is close to the freezing point.

B. Calculation of three- and four-body direct correlation functions

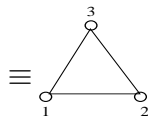
The higher-body direct correlation function is related to the derivatives $\partial^m c^{(0)}(r)/\partial \rho^m$ as follows [2]:

$$\frac{\partial c^{(0)}(r, \rho_0)}{\partial \rho} = \int d\vec{r}_3 \quad c_3^{(0)}(\vec{r}_1, \vec{r}_2, \vec{r}_3; \rho_0), \quad (2.21)$$

$$\begin{aligned}\frac{\partial^2 c^{(0)}(r, \rho_0)}{\partial \rho^2} &= \int d\vec{r}_3 \frac{c_3^{(0)}(\vec{r}_1, \vec{r}_2, \vec{r}_3; \rho_0)}{\partial \rho} \\ &= \int d\vec{r}_3 \int d\vec{r}_4 c_4^{(0)}(\vec{r}_1, \vec{r}_2, \vec{r}_3, \vec{r}_4; \rho_0),\end{aligned}\quad (2.22)$$

etc., where $c_m^{(0)}$ are m-body direct correlation function of the isotropic phase of density ρ_0 . These equations can be solved to find values of $c_m^{(0)}$ by writing them as a product of pair functions. For $c_3^{(0)}(\vec{r}_1, \vec{r}_2, \vec{r}_3)$ one can write as [6],

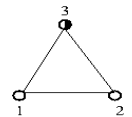
$$c_3^{(0)}(\vec{r}_1, \vec{r}_2, \vec{r}_3) = t(r_{12})t(r_{13})t(r_{23}),$$



$$\equiv \quad (2.23)$$

where a line linking particles i and j denotes a $t(r)$ function and each circle (representing a particle) carry weight unity. The value of $t(r)$ is found from the relation (2.21),

$$\frac{\partial c^{(0)}(r, \rho_0)}{\partial \rho} =$$



$$\quad (2.24)$$

where the half-black circle represents the particle over which integration is performed over its all configurations and all circles carry weight unity. Using known values of $\partial c^{(0)}(r, \rho_0)/\partial \rho_0$ we solve this equation to find values of $t(r)$ for different density ρ_0 (or γ) following a method outlined in ref [6]. The values of $t(r)$ as a function of r are shown in Fig. 2 for $n = 6, 4$ and $\gamma = 2.30, 5.60$, respectively .

Taking derivative of both sides of Eq.(2.23) with respect to ρ_0 one gets,

$$\frac{\partial c_3^{(0)}(\vec{r}_1, \vec{r}_2, \vec{r}_3)}{\partial \rho_0} = \frac{\partial t(r_{12})}{\partial \rho_0} t(r_{13}) t(r_{23}) + t(r_{12}) \frac{\partial t(r_{13})}{\partial \rho_0} t(r_{23}) + t(r_{12}) t(r_{13}) \frac{\partial t(r_{23})}{\partial \rho_0}. \quad (2.25)$$

Substitution of this in Eq.(2.22) leads to

$$\frac{\partial^2 c^{(0)}(r)}{\partial \rho_0^2} = \int d\vec{r}' \left[\frac{\partial t(r)}{\partial \rho_0} t(r') t(|\vec{r}' - \vec{r}|) + t(r) \frac{\partial t(r')}{\partial \rho_0} t(|\vec{r}' - \vec{r}|) + t(r) t(r') \frac{\partial t(|\vec{r}' - \vec{r}|)}{\partial \rho_0} \right], \quad (2.26)$$

where $r_{12} = r$, $r_{13} = r'$ and $r_{23} = |\vec{r}' - \vec{r}|$. As values of $t(r)$ are known, Eq.(2.26) is used to find values of $\partial t(r)/\partial \rho_0$ in same way as Eq.(2.24) was used to find values of $t(r)$. In Fig. 3 we plot $\partial t(r)/\partial \rho_0$ for $n = 4, 6$ and $\gamma = 5.60, 2.30$.

Guided by the relation of Eq.(2.24) we write $\partial t(r)/\partial \rho_0$ as

$$\frac{\partial t(r)}{\partial \rho} = s(r) \int d\vec{r}'' s(r'') s(|\vec{r}'' - \vec{r}|),$$

$$\equiv \begin{array}{c} \bullet \\ \diagup \quad \diagdown \\ \circ_1 \quad \circ_2 \end{array} \quad (2.27)$$

where a dashed line connecting particles i and j is $s(r)$ function. Using the already determined values of $\partial t(r)/\partial \rho_0$ at a given value of ρ_0 (or γ) we determine values of $s(r)$ in same way as values of $t(r)$ were determined from known values of $\partial c^{(0)}(r)/\partial \rho_0$. In Fig. 4 we plot values of $s(r)$ for $n = 6, 4$ and $\gamma = 2.30, 5.60$ as a function of r .

From Eqs.(2.22), (2.25) and (2.27) we get

$$c_4^{(0)}(\vec{r}_1, \vec{r}_2, \vec{r}_3, \vec{r}_4) = \begin{array}{c} \circ_4 \\ \diagdown \quad \diagup \\ \circ_1 \quad \circ_2 \end{array} + \begin{array}{c} \circ_4 \\ \diagdown \quad \diagup \\ \circ_1 \quad \circ_2 \end{array} + \begin{array}{c} \circ_3 \\ \diagdown \quad \diagup \\ \circ_1 \quad \circ_2 \end{array}, \quad (2.28)$$

where a dashed line represents $s(r)$ -bond and a full line $t(r)$ -bond. We calculate values of $c_3^{(0)}$ and $c_4^{(0)}$ and plot them in Appendix.

C. Evaluation of $c^{(b)}(\vec{r}_1, \vec{r}_2)$

The function $c^{(b)}(\vec{r}_1, \vec{r}_2)$ can be expanded in ascending powers of $(\rho(\vec{r}) - \rho_0)$ as [2, 13],

$$\begin{aligned} c^{(b)}(\vec{r}_1, \vec{r}_2; [\rho]) &= \int d\vec{r}_3 c_3^{(0)}(\vec{r}_1, \vec{r}_2, \vec{r}_3; \rho_0) (\rho(\vec{r}_3) - \rho_0) \\ &+ \frac{1}{2} \int d\vec{r}_3 \int d\vec{r}_4 c_4^{(0)}(\vec{r}_1, \vec{r}_2, \vec{r}_3, \vec{r}_4; \rho_0) (\rho(\vec{r}_3) - \rho_0) (\rho(\vec{r}_4) - \rho_0) \\ &+ \dots \quad , \end{aligned} \quad (2.29a)$$

$$\equiv \begin{array}{c} \bullet \\ \diagup \quad \diagdown \\ \circ_1 \quad \circ_2 \end{array} + \frac{1}{2} \begin{array}{c} \bullet \\ \diagup \quad \diagdown \\ \circ_1 \quad \circ_2 \\ \bullet \\ \diagup \quad \diagdown \\ \circ_1 \quad \circ_2 \end{array} + \frac{1}{2} \begin{array}{c} \bullet \\ \diagup \quad \diagdown \\ \circ_1 \quad \circ_2 \\ \bullet \\ \diagup \quad \diagdown \\ \circ_1 \quad \circ_2 \end{array} + \frac{1}{2} \begin{array}{c} \bullet \\ \diagup \quad \diagdown \\ \circ_1 \quad \circ_2 \\ \bullet \\ \diagup \quad \diagdown \\ \circ_1 \quad \circ_2 \end{array} + \dots \quad (2.29b)$$

where black circles represent integration over all configurations of these particles and each carries weight $\rho(\vec{r}_i) - \rho_0 = \sum_G \rho_G e^{i\vec{G} \cdot \vec{r}_i}$ whereas each white circle carries weight unity. In writing Eq.(2.29b) use has been made of Eqs.(2.23) and (2.28).

Usefulness of series of Eq.(2.29) depends on how fast it converges and on our ability of finding values of $c_m^{(0)}$. We have already described the calculation of $c_3^{(0)}$ and $c_4^{(0)}$. The same procedure can be used to find $c_m^{(0)}$ for $m > 4$. We, however, find that for a wide range of potentials it is enough to consider the first two terms of the series (2.29). In fact, for most potentials representing the inter-particle interactions in real systems one may need to consider the first term only as contribution made by the second term to the grand thermodynamic potential at the freezing point turns out to be negligibly small unless the potential has a long range tail.

1. Evaluation of first term of Eq.(2.29)

Substituting value of $(\rho(\vec{r}_3) - \rho_0)$ from Eq.(2.3) and using notations, $\vec{r} = \vec{r}_2 - \vec{r}_1$, $\vec{r}' = \vec{r}_3 - \vec{r}_1$, $\vec{r}_c = \frac{1}{2}(\vec{r}_1 + \vec{r}_2)$ we find

$$\begin{array}{c} \bullet \\ \diagup \quad \diagdown \\ \circ_1 \quad \circ_2 \end{array} \equiv c^{(b,1)}(\vec{r}_1, \vec{r}_2) = \sum_G \rho_G e^{i\vec{G} \cdot \vec{r}_c} t(r) e^{-\frac{1}{2}i\vec{G} \cdot \vec{r}} \int d\vec{r}' t(r') t(|\vec{r}' - \vec{r}|) e^{i\vec{G} \cdot \vec{r}'}. \quad (2.30)$$

This is solved to give [13, 14]

$$c^{(b,1)}(\vec{r}_1, \vec{r}_2) = \sum_G e^{i\vec{G} \cdot \vec{r}_c} \sum_{lm} c_l^{(G,1)}(r) Y_{lm}(\hat{r}) Y_{lm}^*(\hat{G}), \quad (2.31)$$

where

$$c_l^{(G,1)}(r) = \rho_G \sum_{l_1} \sum_{l_2} \Lambda_1(l_1, l_2, l) j_{l_2} \left(\frac{1}{2} Gr \right) B_{l_1}(r, G). \quad (2.32)$$

Here $j_l(x)$ is the spherical Bessel function, $Y_{lm}(\hat{x})$ the spherical harmonics,

$$\Lambda_1(l_1, l_2, l) = (i)^{l_1+l_2} (-1)^{l_2} \left[\frac{(2l_1+1)(2l_2+1)}{(2l+1)} \right]^{\frac{1}{2}} [C_g(l_1, l_2, l; 0, 0, 0)]^2, \quad (2.33)$$

and

$$B_{l_1}(r, G) = 8t(r) \int dk k^2 t(k) j_{l_1}(kr) \int dr' r'^2 t(r') j_{l_1}(kr') j_{l_1}(Gr'), \quad (2.34)$$

where C_g is the Clebsch-Gordan coefficient. The crystal symmetry dictates that l and $l_1 + l_2$ are even and for a cubic crystal, $m = 0, \pm 4$.

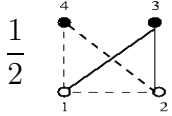
The values of $c_i^{(G,1)}(r)$ depend on order parameters $\rho_G = \rho_0 \mu_G$, where $\mu_G = e^{-G^2/4\alpha}$ and on magnitude of \vec{G} . In Figs. 5, 6 we plot and compare values of $c_i^{(G,1)}(r)$ for bcc and fcc crystals at the melting point for potential $n = 6$, $\gamma_s = 2.32$, $\alpha_{bcc} = 18$ and $\alpha_{fcc} = 32$ (see Table I). The values given in these figures are for the first and second sets of RLV's. As expected, the values are far from negligible and differ considerably for the two structures. The value is found to decrease rapidly as the value of l is increased; the maximum contribution comes from $l = 0$. We also find, as shown in Fig. 7, the value of $c_i^{(G,1)}(r)$ decreases rapidly as the magnitude of \vec{G} vector increases; the maximum contribution comes from the first two sets of RLV's. The other point to be noted is that at a given point r , values of $c_i^{(G,1)}(r)$ are positive for some \vec{G} vectors while for others the values are negative leading to mutual cancellation in a quantity where summation over \vec{G} is involved.

2. Evaluation of second term of Eq.(2.29)

The contribution arising from the second term of Eq.(2.29) is sum of three diagrams in which the last two contributions are equal. Thus,

$$c^{(b,2)}(\vec{r}_1, \vec{r}_2) = \frac{1}{2} \left[\begin{array}{c} \bullet 4 \quad \bullet 3 \\ \diagdown \quad \diagup \\ \circ 1 \quad \circ 2 \end{array} + \begin{array}{c} \bullet 4 \quad \bullet 3 \\ \diagdown \quad \diagup \\ \circ 1 \quad \circ 2 \end{array} \right]. \quad (2.35)$$

If we write $\vec{r}'' = \vec{r}_4 - \vec{r}_1$ and $\vec{r}_4 = \vec{r}'' + \vec{r}_c - \frac{1}{2}\vec{r}$ and use other notations defined above, the first diagram can be written as



$$\frac{1}{2} \equiv c^{(b,2,1)}(\vec{r}_1, \vec{r}_2) = \frac{1}{2} s(r) \sum_{G_1} \sum_{G_2} \rho_{G_1} \rho_{G_2} e^{i(\vec{G}_1 + \vec{G}_2) \cdot (\vec{r}_c - \frac{1}{2} \vec{r})} \int d\vec{r}' t(r') t(|\vec{r}' - \vec{r}|) e^{i\vec{G}_1 \cdot \vec{r}'} \int d\vec{r}'' s(r'') s(|\vec{r}'' - \vec{r}|) e^{i\vec{G}_2 \cdot \vec{r}''}. \quad (2.36)$$

This is solved to give

$$c^{(b,2,1)}(\vec{r}_1, \vec{r}_2) = \sum_G e^{i\vec{G} \cdot \vec{r}_c} \sum_{lm} \sum_{l'm'} c_{lm, l'm'}^{(G,2,1)}(r) Y_{l'm'}^*(\hat{G}) Y_{lm}(\hat{r}), \quad (2.37)$$

where

$$c_{lm, l'm'}^{(G,2,1)}(r) = \sum_{G_1} \rho_{G_1} \rho_K \sum_{l_1 m_1} \sum_{l_2 m_2} \Lambda_{mm' m_1 m_2}^{l' l_1 l_2} M_{l_1}(r, G_1) M_{l_2}(r, K) j_{l'} \left(\frac{1}{2} Gr \right) Y_{l_1 m_1}^*(\hat{G}_1) Y_{l_2 m_2}^*(\hat{K}). \quad (2.38)$$

$$\text{Here } \vec{K} = \vec{G} - \vec{G}_1,$$

$$\Lambda_{mm' m_1 m_2}^{l' l_1 l_2} = 16 \sum_{l_3 m_3} (i)^{l_1 + l_2 + l'} (-1)^{l'} \left[\frac{(2l_1 + 1)(2l_2 + 1)(2l' + 1)}{(2l + 1)} \right]^{1/2} C_g(l_1, l_2, l_3; 0, 0, 0) C_g(l', l_3, l; 0, 0, 0) C_g(l_1, l_2, l_3; m_1, m_2, m_3) C_g(l', l_3, l; m', m_3, m); \quad (2.39)$$

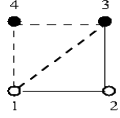
$$M_{l_1}(r, G_1) = \int dr' r'^2 j_{l_1}(Gr') t(r') \int dk k^2 t(k) j_{l_1}(kr) j_{l_1}(kr') \quad (2.40)$$

and

$$M_{l_2}(r, K) = \int dr'' r''^2 j_{l_2}(Kr'') s(r'') \int dk k^2 s(k) j_{l_2}(kr) j_{l_2}(kr'') \quad (2.41)$$

The crystal symmetry dictates that all l_i are even and for a cubic crystal all m_i are 0 and ± 4 .

From the second diagram of Eq.(2.35) we get



$$\equiv c^{(b,2,2)}(\vec{r}_1, \vec{r}_2) = t(r) \sum_{G_1} \sum_{G_2} \rho_{G_1} \rho_{G_2} e^{i(\vec{G}_1 + \vec{G}_2) \cdot (\vec{r}_c - \frac{1}{2}\vec{r})}$$

$$\int d\vec{r}' s(r') t(|\vec{r}' - \vec{r}|) e^{i\vec{G}_1 \cdot \vec{r}'} \int d\vec{r}'' s(r'') s(|\vec{r}'' - \vec{r}'|) e^{i\vec{G}_1 \cdot \vec{r}''}. \quad (2.42)$$

This is solved to give

$$c^{(b,2,2)}(\vec{r}_1, \vec{r}_2) = \sum_G e^{i\vec{G} \cdot \vec{r}_c} \sum_{lm} \sum_{l'm'} c_{lm, l'm'}^{(G,2,2)}(r) Y_{l'm'}^*(\hat{G}) Y_{lm}(\hat{r}), \quad (2.43)$$

where

$$c_{lm, l'm'}^{(G,2,2)}(r) = \sum_{G_1} \rho_{G_1} \rho_K \sum_{l_1 m_1} \sum_{l_2 m_2} \sum_{l_3 m_3} \Lambda_{mm' m_1 m_2 m_3}^{l' l_1 l_2 l_3} N_{l_1, l_2, l_3}(r, G, G_1)$$

$$j_{l'} \left(\frac{1}{2} Gr \right) Y_{l_1 m_1}^*(\hat{G}_1) Y_{l_2 m_2}^*(\hat{K}), \quad (2.44)$$

$$\Lambda_{mm' m_1 m_2 m_3}^{l' l_1 l_2 l_3} = 32(i)^{l_1 + l_2 + l'} (-1)^{l'} \left[\frac{(2l_1 + 1)(2l_2 + 1)(2l' + 1)}{(2l + 1)} \right]^{1/2}$$

$$C_g(l_1, l_2, l_3; 0, 0, 0) C_g(l', l_3, l; 0, 0, 0) C_g(l_1, l_2, l_3; m_1, m_2, m_3) C_g(l', l_3, l; m', m_3, m); \quad (2.45)$$

$$N_{l_1, l_2, l_3}(r, G, G_1) = t(r) \int dr' r'^2 s(r') j_{l_1}(G_1 r') B_{l_2}(r', K) A_{l_3}(r, r'), \quad (2.46)$$

$$A_{l_3}(r, r') = \int dk k^2 t(k) j_{l_3}(kr) j_{l_3}(kr') \quad (2.47)$$

and

$$B_{l_2}(r', K) = \int dr'' r''^2 j_{l_2}(K r'') s(r'') \int dk k^2 s(k) j_{l_2}(kr') j_{l_2}(kr''). \quad (2.48)$$

The total contribution arising from the second term of Eq.(2.29) is

$$c^{(b,2)}(\vec{r}_1, \vec{r}_2) = \sum_G e^{i\vec{G}\cdot\vec{r}_c} \sum_{lm} \sum_{l'm'} \left[c_{lm'l'm'}^{(G,2,1)}(r) + c_{lm'l'm'}^{(G,2,2)}(r) \right] Y_{lm}(\hat{r}) Y_{l'm'}^*(\hat{G}), \quad (2.49)$$

where l, l' are even and $m = 0, \pm 4$ for cubic lattices. In Figs. 8 and 9 we plot values of

$$c_{lm'l'm'}^{(G,2)}(r) = c_{lm'l'm'}^{(G,2,1)}(r) + c_{lm'l'm'}^{(G,2,2)}(r), \quad (2.50)$$

as a function of r for bcc and fcc structures for $n = 6$, $\gamma_s = 2.32$, $\alpha_{bcc} = 18$ and $\alpha_{fcc} = 32$. The values given in these figures are for the first two sets of RLV's for $l = l' = 0$ and 2, and $m = m' = 0$. These are the terms which mostly contribute to $c_{lm'l'm'}^{(G,2)}(r)$; the contributions from terms $l \neq l'$ and $m \neq m'$ are approximately order of magnitude smaller. For a bcc lattice we find two sets of values; one for \vec{G} vectors lying in the x-y plane and the other for the rest of the vectors. Since all vectors of the first set of RLV's of a fcc lattice are out of x-y plane we get only one set of values. For the second set of RLV's of a fcc lattice, though two sets of values are found but they are close unlike the case of bcc lattice where the two sets of values differ not only in magnitude but also in sign. The values differ considerably for the two cubic structures. The value of $c_{lm'l'm'}^{(G,2)}(r)$ decreases for both bcc and fcc structures rapidly as the magnitude of \vec{G} vectors increases as was found in the case of $c_l^{(G,1)}(r)$. Furthermore, the values of $c_{lm'l'm'}^{(G,2)}(r)$ at a given value of r is positive for some \vec{G} vector and negative for others.

In order to compare magnitude of contributions made by the first and second terms of Eq.(2.29) we calculate $\hat{c}^{(G,1)}(k, \theta_k, \phi_k)$ and $\hat{c}^{(G,2)}(k, \theta_k, \phi_k)$ defined as

$$\begin{aligned} \hat{c}^{(G,1)}(k, \theta_k, \phi_k) &= \rho \sum_{lm} \int d\vec{r} c_l^{(G,1)}(r) e^{i\vec{k}\cdot\vec{r}} Y_{lm}(\hat{r}) Y_{lm}^*(\hat{G}) \\ &= 4\pi \rho \sum_{lm} (i)^l Y_{lm}(\hat{k}) Y_{lm}^*(\hat{G}) \int_0^\infty dr r^2 c_l^{(G,1)}(r) j_l(kr) \end{aligned} \quad (2.51)$$

and

$$\begin{aligned} \hat{c}^{(G,2)}(k, \theta_k, \phi_k) &= \rho \sum_{lm} \sum_{l'm'} \int d\vec{r} c_{lm'l'm'}^{(G,2)}(r) e^{i\vec{k}\cdot\vec{r}} Y_{lm}(\hat{r}) Y_{l'm'}^*(\hat{G}) \\ &= 4\pi \rho \sum_{lm} \sum_{l'm'} (i)^l Y_{lm}(\hat{k}) Y_{l'm'}^*(\hat{G}) \int_0^\infty dr r^2 c_{lm'l'm'}^{(G,2)}(r) j_l(kr). \end{aligned} \quad (2.52)$$

In Figs. 10 and 11 we compare using colour codes (shown on the right hand side of each figure) the values of these functions arising from the first and second terms of Eq.(2.29) for both fcc and bcc structures for $n = 6$, $\gamma_s = 2.32$, $\alpha_{fcc} = 32$ and $\alpha_{bcc} = 18$. The values given in Fig. 10 are for a fcc lattice for a \vec{G} vector of first and a vector of second sets, i.e. $G_1 a_0 = 4.25$, $\theta_{G_1} = 54.7^\circ$ and $\phi_{G_1} = 45^\circ$ and $G_2 a_0 = 4.91$, $\theta_{G_2} = 0^\circ$, $\phi_{G_2} = 90^\circ$. The values of ka_0 are taken equal to 4.25, 4.91 which are magnitude of $G_1 a_0$ and $G_2 a_0$, respectively. In Fig. 11 we compare the values of $c^{(G,1)}(k, \theta_k, \phi_k)$ and $c^{(G,2)}(k, \theta_k, \phi_k)$ for a bcc lattice for $G_1 a_0 = 4.37$, $\theta_{G_1} = 90^\circ$, $\phi_{G_1} = 45^\circ$ and $G_2 a_0 = 6.19$, $\theta_{G_2} = 90^\circ$, $\phi_{G_2} = 0^\circ$ and $ka_0 = 4.37$ and 6.19. From these figures it is clear that the contribution made by the second term to $c^{(b)}(\vec{r}_1, \vec{r}_2)$ is small compared to the first term indicating fast convergence of the series. As is shown below, in the expression of free energy functional, $c^{(b)}(\vec{r}_1, \vec{r}_2)$ is averaged over density and order parameters and also there is summation over \vec{G} vectors, As a consequence, the contribution of second term of Eq.(2.29) is found to be order of magnitude smaller than the first term. We show that the consideration of the first two terms of Eq.(2.29) is enough to give accurate description of freezing transitions for a wide class of potentials.

III. FREE-ENERGY FUNCTIONAL AND LIQUID-SOLID TRANSITION

The reduced free-energy functional $A[\rho]$ of a symmetry broken phase can be written as [13, 14, 17]

$$A[\rho] = A_{id}[\rho] + A_{ex}^{(0)}[\rho] + A_{ex}^{(b)}[\rho] \quad (3.1)$$

where

$$A_{id}[\rho] = \int d\vec{r} \rho(\vec{r}) [\ln(\rho(\vec{r})\Lambda) - 1] \quad (3.2)$$

$$\begin{aligned} A_{ex}^{(0)}[\rho] &= A_{ex}(\rho_l) + \beta(\mu - \ln(\rho_l\Lambda)) \int d\vec{r} (\rho(\vec{r}) - \rho_l) \\ &\quad - \frac{1}{2} \int d\vec{r}_1 \int d\vec{r}_2 (\rho(\vec{r}_1) - \rho_l)(\rho(\vec{r}_2) - \rho_l) \bar{c}^{(0)}(|\vec{r}_2 - \vec{r}_1|) \end{aligned} \quad (3.3)$$

and

$$A_{ex}^{(b)}[\rho] = -\frac{1}{2} \int d\vec{r}_1 \int d\vec{r}_2 (\rho(\vec{r}_1) - \rho_0)(\rho(\vec{r}_2) - \rho_0) \bar{c}^{(b)}(\vec{r}_1, \vec{r}_2) \quad (3.4)$$

Here Λ is cube of the thermal wavelength associated with a molecule, $\beta = (k_B T)^{-1}$, k_B being the Boltzmann constant and T is the temperature, $A_{ex}^{(0)}(\rho_l)$ is excess reduced free energy of the coexisting isotropic liquid of density ρ_l and chemical potential μ and $\rho_0 = \rho_l (1 + \Delta\rho^*)$ is the average density of the solid.

$$\bar{c}^{(0)}(|\vec{r}_2 - \vec{r}_1|) = 2 \int_0^1 d\lambda \lambda \int_0^1 d\lambda' c^{(0)}(|\vec{r}_2 - \vec{r}_1|; \rho_l + \lambda\lambda'(\rho_0 - \rho_l)) \quad (3.5)$$

and

$$\bar{c}^{(b)}(\vec{r}_1, \vec{r}_2) = 4 \int_0^1 d\lambda \lambda \int_0^1 d\lambda' \int_0^1 d\xi \xi \int_0^1 d\xi' c^{(b)}(\vec{r}_1, \vec{r}_2; \lambda\lambda' \rho_0, \xi\xi' \rho_G) \quad (3.6)$$

The expression for the symmetry conserving part of reduced excess free energy $A_{ex}^{(0)}[\rho]$ given by Eq.(3.3) is found by performing double functional integration of [13, 17]

$$\frac{\delta^2 A_{ex}^{(0)}[\rho]}{\delta\rho(\vec{r}_1) \delta\rho(\vec{r}_2)} = -c^{(0)}(|\vec{r}_2 - \vec{r}_1|). \quad (3.7)$$

This integration is carried out in the density space taking the coexisting uniform fluid of density ρ_l and chemical potential μ as a reference. The expression for the symmetry broken part $A_{ex}^{(b)}[\rho]$ given by Eq.(3.4) is found by performing double functional integration of [13, 17]

$$\frac{\delta^2 A_{ex}^{(b)}[\rho]}{\delta\rho(\vec{r}_1) \delta\rho(\vec{r}_2)} = -c^{(b)}(\vec{r}_1, \vec{r}_2), \quad (3.8)$$

in the density space corresponding to the symmetry broken phase. The path of integration in this space is characterized by two parameters λ and ξ . These parameters vary from 0 to 1. The parameter λ raises the density from zero to the final value ρ_0 as it varies from 0 to 1, whereas parameter ξ raises the order parameter from 0 to its final value ρ_G . The result is independent of the order of integration.

In locating the transition the grand thermodynamic potential defined as

$$-W = A - \beta\mu \int d\vec{r} \rho(\vec{r}) \quad (3.9)$$

is generally used as it ensures the pressure and chemical potential of both phases remain equal at the transition. The transition point is determined by the condition $\Delta W = W_l - W = 0$,

where W_l is the grand thermodynamic potential of the co-existing liquid. The expression of ΔW is found to be [13, 14]

$$\begin{aligned} \Delta W = & \int d\vec{r} \left[\rho(\vec{r}) \ln \left(\frac{\rho(\vec{r})}{\rho_l} \right) - (\rho(\vec{r}) - \rho_l) \right] \\ & - \frac{1}{2} \int d\vec{r}_1 \int d\vec{r}_2 (\rho(\vec{r}_1) - \rho_l) (\rho(\vec{r}_2) - \rho_l) \tilde{c}^{(0)}(|\vec{r}_2 - \vec{r}_1|) \\ & - \frac{1}{2} \int d\vec{r}_1 \int d\vec{r}_2 (\rho(\vec{r}_1) - \rho_0) (\rho(\vec{r}_2) - \rho_0) \tilde{c}^{(b)}(\vec{r}_1, \vec{r}_2). \end{aligned} \quad (3.10)$$

Minimization of ΔW with respect to $\rho(\vec{r})$ subject to the perfect crystal constraint leads to

$$\ln \frac{\rho(\vec{r}_1)}{\rho_l} = \phi + \int d\vec{r}_2 (\rho(\vec{r}_2) - \rho_l) \tilde{c}^{(0)}(|\vec{r}_2 - \vec{r}_1|) + \int d\vec{r}_2 (\rho(\vec{r}_2) - \rho_0) \tilde{c}^{(b)}(\vec{r}_1, \vec{r}_2), \quad (3.11)$$

where

$$\tilde{c}^{(0)}(|\vec{r}_2 - \vec{r}_1|) = \int_0^1 d\lambda c^{(0)}(|\vec{r}_2 - \vec{r}_1|; \rho_l + \lambda(\rho_0 - \rho_l))$$

and

$$\tilde{c}^{(b)}(\vec{r}_1, \vec{r}_2) = \int_0^1 d\lambda \int_0^1 d\xi c^{(b)}(\vec{r}_1, \vec{r}_2; \lambda\rho_0, \xi\rho_G)$$

The value of the Lagrange multiplier ϕ in Eq.(3.11) is found from the condition

$$\frac{1}{V} \int d\vec{r} \frac{\rho(\vec{r})}{\rho_0} = 1 \quad (3.12)$$

where V is volume of the system.

It may be noted that, in principle, one needs only values of symmetry conserved and symmetry broken parts of the DPCF to determine $\rho(\vec{r})$ that minimizes the grand potential W . In practice, however, it is found convenient to do minimization with respect to an assumed form of $\rho(\vec{r})$. The ideal part is calculated using a form of $\rho(\vec{r})$ which is a superposition of normalized Gaussians centred around the lattice sites,

$$\rho(\vec{r}) = \left(\frac{\alpha}{\pi}\right)^{3/2} \sum_n \exp \left[-\alpha \left(\vec{r} - \vec{R}_i \right)^2 \right] \quad (3.13)$$

where α is the variational parameter that characterizes the width of the Gaussian; the square root of α is inversely proportional to the width of a peak. It thus measures the non-uniformity; $\alpha = 0$ corresponds to the limit of a uniform liquid and an increasing value of α corresponds to increasing localization of particles on their respective lattice sites defined by vectors \vec{R}_i . For the interaction part it is convenient to use the expression of $\rho(\vec{r})$ given by Eq.(2.3). The Fourier transform of Eq.(3.13) leads to $\rho_G = \rho_0 \mu_G$, where $\mu_G = e^{-G^2/4\alpha}$.

A. Evaluation of $\bar{c}^{(0)}(r)$ and $\bar{c}^{(b)}(\vec{r}_1, \vec{r}_2)$

The values of $\bar{c}^{(0)}(r)$ for a given liquid density ρ_l and the average crystal density ρ_0 are found from the known values of $c^{(0)}(r, \rho)$ where ρ varies from ρ_l to ρ_0 by performing integrations in Eq.(3.5) which can be rewritten as

$$\bar{c}^{(0)}(r, \rho_0) = 2 \int_0^1 d\lambda \lambda \int_0^1 d\lambda' c^{(0)} \left(r; \rho_l (1 + \lambda \lambda' \Delta \rho^*) \right) \quad (3.14)$$

where $\Delta \rho^* = (\rho_0 - \rho_l)/\rho_l$. The integrations have been done numerically using a very fine grid for variables λ and λ' . Since at the freezing point $\rho_l \Delta \rho^* \ll 1$ one can use Taylor expansion to solve Eq.(3.14) leading to

$$\bar{c}^{(0)}(r, \rho_0) = c^{(0)}(r, \rho_l) + \frac{1}{3} \rho_l \Delta \rho^* \frac{\partial c^{(0)}(r, \rho_l)}{\partial \rho_l} + O(\rho_l^2 \Delta \rho^{*2}) \quad (3.15)$$

Since the order parameters that appear in $\bar{c}^{(b)}(\vec{r}_1, \vec{r}_2)$ are linear in $c^{(b,1)}(\vec{r}_1, \vec{r}_2)$ and quadratic in $c^{(b,2)}(\vec{r}_1, \vec{r}_2)$, the integration over ξ variables in Eq.(3.4) can be performed analytically leading to

$$\begin{aligned} \bar{c}^{(b)}(\vec{r}_1, \vec{r}_2) = \sum_G e^{i\vec{G} \cdot \vec{r}_c} \left[\sum_{lm} \bar{c}_l^{(G,1)}(r) Y_{lm}^*(\hat{G}) Y_{lm}(\hat{r}) \right. \\ \left. + \sum_{lm} \sum_{l'm'} \left(\bar{c}_{lm,l'm'}^{(G,2,1)}(r) + \bar{c}_{lm,l'm'}^{(G,2,2)}(r) \right) Y_{l'm'}^*(\hat{G}) Y_{lm}(\hat{r}) \right] \quad (3.16) \end{aligned}$$

where

$$\bar{c}_l^{(G,1)}(r) = \frac{1}{3}\rho_G \sum_{l_1} \sum_{l_2} \Lambda_1(l_1, l_2, l) j_{l_2} \left(\frac{1}{2}Gr \right) \bar{B}_{l_1}(r, G), \quad (3.17)$$

$$\begin{aligned} \bar{c}_{lm, l'm'}^{(G,2,1)}(r) = \frac{1}{6} \sum_{G_1} \rho_{G_1} \rho_K \sum_{l_1 m_1} \sum_{l_2 m_2} \Lambda_{mm'/m_1 m_2}^{l'l_1 l_2} j_l \left(\frac{1}{2}Gr \right) \\ \bar{Q}_{l_1 l_2}(r, G, G_1) Y_{l_1 m_1}^*(\hat{G}_1) Y_{l_2 m_2}^*(\hat{K}), \end{aligned} \quad (3.18)$$

$$\begin{aligned} \bar{c}_{lm, l'm'}^{(G,2,2)}(r) = \frac{1}{6} \sum_{G_1} \rho_{G_1} \rho_K \sum_{l_1 m_1} \sum_{l_2 m_2} \sum_{l_3 m_3} \Lambda_{mm'/m_1 m_2 m_3}^{l'l_1 l_2 l_3} j_{l'} \left(\frac{1}{2}Gr \right) \\ \bar{N}_{l_1 l_2 l_3}(r, G, G_1) Y_{l_2 m_2}^*(\hat{G}_1) Y_{l_3 m_3}^*(\hat{K}), \end{aligned} \quad (3.19)$$

with

$$\bar{B}_{l_1}(r, G) = 2 \int_0^1 d\lambda \lambda \int_0^1 d\lambda' B_{l_1} \left(r, G; \lambda \lambda' \rho \right), \quad (3.20)$$

$$\bar{Q}_{l_1 l_2}(r, G, G_1) = 2 \int_0^1 d\lambda \lambda \int_0^1 d\lambda' Q_{l_1 l_2} \left(r, G, G_1; \lambda \lambda' \rho \right), \quad (3.21)$$

$$Q_{l_1 l_2} \left(r, G, G_1; \rho \right) = M_{l_1} \left(r, G_1; \rho \right) M_{l_2} \left(r, K; \rho \right),$$

and

$$\bar{N}_{l_1 l_2 l_3}(r, G, G_1) = 2 \int_0^1 d\lambda \lambda \int_0^1 d\lambda' N_{l_1 l_2 l_3} \left(r, G, G_1; \lambda \lambda' \rho \right). \quad (3.22)$$

The quantities $B_{l_1}(r, G)$, $M_{l_1}(r, G_1)$, $M_{l_2}(r, K)$ and $N_{l_1 l_2 l_3}(r, G, G_1)$ are defined by Eqs. (2.34), (2.40), (2.41) and (2.46) respectively. The integrations over λ and λ' have been performed numerically by varying them from 0 to 1 on a fine grid and evaluating the functions B_{l_1} , $Q_{l_1 l_2}$ and $N_{l_1 l_2 l_3}$ on these densities. Since these functions vary smoothly with density and their values have been evaluated at closely spaced values of density the result found for $\bar{c}^{(b)}(\vec{r}_1, \vec{r}_2)$ is expected to be accurate.

B. Evaluation of ΔW

Substituting expression of $\rho(\vec{r})$ given by Eqs.(2.3) and (3.14) and of $\bar{c}^{(0)}(r)$ and $\bar{c}^{(b)}(\vec{r}_1, \vec{r}_2)$ given above in Eq.(3.10) we find

$$\frac{\Delta W}{N} = \frac{\Delta W_{id}}{N} + \frac{\Delta W_0}{N} + \frac{\Delta W_b^{(1)}}{N} + \frac{\Delta W_b^{(2)}}{N} \quad (3.23)$$

where

$$\frac{\Delta W_{id}}{N} = 1 - (1 + \Delta\gamma) \left[\frac{5}{2} + \ln \rho_l - \frac{3}{2} \ln \left(\frac{\alpha}{\pi} \right) \right] \quad (3.24)$$

$$\frac{\Delta W_0}{N} = -\frac{1}{2} \Delta\gamma \widehat{c}^{(0)}(0) - \frac{1}{2} (1 + \Delta\gamma)^2 \sum_{G \neq 0} |\mu_G|^2 \widehat{c}^{(0)}(G) \quad (3.25)$$

$$\frac{\Delta W_b^{(1)}}{N} = -\frac{1}{2} \rho_l (1 + \Delta\gamma)^2 \sum'_G \sum'_{G_2} \mu_{G_2} \mu_{-G-G_2} \widehat{c}^{(G,1)} \left(\vec{G}_2 + \frac{1}{2} \vec{G} \right) \quad (3.26)$$

$$\frac{\Delta W_b^{(2)}}{N} = -\frac{1}{2} \rho_l (1 + \Delta\gamma)^2 \sum'_G \sum'_{G_2} \mu_{G_2} \mu_{-G-G_2} \widehat{c}^{(G,2)} \left(\vec{G}_2 + \frac{1}{2} \vec{G} \right) \quad (3.27)$$

where $\Delta\gamma = (\gamma_s - \gamma_l) / \gamma_l$; the subscripts s and l stand for solid and liquid, respectively. Here ΔW_{id} , ΔW_0 , $\Delta W_b^{(1)}$ and $\Delta W_b^{(2)}$ are respectively, the ideal, symmetry conserving and symmetry broken contributions from first and second terms of series (2.29) to ΔW . The prime on summation in Eqs.(3.26), (3.27) indicates the condition $\vec{G} \neq 0$, $\vec{G}_1 \neq 0$, $\vec{G}_2 \neq 0$, $\vec{G} + \vec{G}_1 \neq 0$ and $\vec{G} + \vec{G}_2 \neq 0$ and

$$\widehat{c}^{(0)}(G) = \int d\vec{r} \bar{c}^{(0)}(r, \gamma_l) e^{i\vec{G} \cdot \vec{r}}, \quad (3.28)$$

$$\begin{aligned} \widehat{c}^{(G,1)} \left(\vec{G}_2 + \frac{1}{2} \vec{G} \right) &= \frac{1}{3} \mu_G \sum_{l_1} \sum_{l_2} \Lambda_1(l_1, l_2, l) Y_{lm}^*(\hat{G}) \int d\vec{r} j_{l_2} \left(\frac{1}{2} Gr \right) \\ &\quad \bar{B}_{l_1}(r, G) e^{i(\vec{G}_2 + \frac{1}{2} \vec{G}) \cdot \vec{r}} Y_{lm}(\hat{r}), \end{aligned} \quad (3.29)$$

$$\hat{c}^{(G,2)} \left(\vec{G}_2 + \frac{1}{2}\vec{G} \right) = \hat{c}^{(G,2,1)} \left(\vec{G}_2 + \frac{1}{2}\vec{G} \right) + 2 \hat{c}^{(G,2,2)} \left(\vec{G}_2 + \frac{1}{2}\vec{G} \right),$$

$$\begin{aligned} \hat{c}^{(G,2,1)} \left(\vec{G}_2 + \frac{1}{2}\vec{G} \right) &= \frac{1}{6} \sum_{G_1} \mu_{G_1} \mu_K \sum_{lm} \sum_{l'm'} \sum_{l_1 m_1} \sum_{l_2 m_2} \sum \Lambda_{mm'l_1 l_2}^{ll'l_1 l_2} Y_{l'm'}^*(\hat{G}) Y_{l_1 m_1}^*(\hat{G}_1) Y_{l_2 m_2}^*(\hat{K}) \\ &\int d\vec{r} j_{l_2} \left(\frac{1}{2}Gr \right) \bar{Q}_{l_1 l_2}(r, G, G_1) e^{i(\vec{G}_2 + \frac{1}{2}\vec{G}) \cdot \vec{r}} Y_{lm}(\hat{r}), \end{aligned} \quad (3.30)$$

$$\begin{aligned} \hat{c}^{(G,2,2)} \left(\vec{G}_2 + \frac{1}{2}\vec{G} \right) &= \frac{1}{6} \sum_{G_1} \mu_{G_1} \mu_K \sum_{lm} \sum_{l'm'} \sum_{l_1 m_1} \sum_{l_2 m_2} \sum_{l_3 m_3} \sum \Lambda_{mm'l_1 l_2 l_3}^{ll'l_1 l_2 l_3} Y_{l'm'}^*(\hat{G}) Y_{l_2 m_2}^*(\hat{G}_1) Y_{l_3 m_3}^*(\hat{K}) \\ &\int d\vec{r} j_{l_2} \left(\frac{1}{2}Gr \right) \bar{N}_{l_1 l_2 l_3}(r, G, G_1) e^{i(\vec{G}_2 + \frac{1}{2}\vec{G}) \cdot \vec{r}} Y_{lm}(\hat{r}). \end{aligned} \quad (3.31)$$

The terms $\frac{\Delta W_0}{N}$, $\frac{\Delta W_b^{(1)}}{N}$ and $\frac{\Delta W_b^{(2)}}{N}$ are respectively second, third and fourth orders in order parameters.

IV. RESULTS FOR LIQUID-CRYSTAL TRANSITION

We use above expression of $\Delta W/N$ to locate the liquid - fcc crystal and the liquid - bcc crystal transitions by varying γ_l , $\Delta\gamma$ and α . For a given γ_l and $\Delta\gamma$, $\Delta W/N$ is minimised with respect to α ; next $\Delta\gamma$ is varied until the lowest value of $\Delta W/N$ at its minimum is found. If this lowest value of $\Delta W/N$ at its minimum is not zero, then γ_l is varied until $\Delta W/N = 0$. The values of transition parameters, γ_l , $\Delta\gamma$ and α for a given lattice structure can also be found from simultaneous solution of equations $\frac{\partial}{\partial(\Delta\gamma)} \left(\frac{\Delta W}{N} \right) = 0$, $\frac{\partial}{\partial\alpha} \left(\frac{\Delta W}{N} \right) = 0$ and $\Delta W/N = 0$.

In Table I we compare values of different terms of $\Delta W/N$ (see Eq.(3.23)) at the freezing point for potentials with $n = 4, 6, 6.5, 7, 12$ and ∞ . The values corresponding to hard spheres are taken from ref.[14]. The contribution made by the symmetry broken part to the grand thermodynamic potential at the freezing point is substantial and its importance increases with the softness of the potential. For example, while for $n = \infty$ the contribution of the symmetry broken part is about 8% of the contribution made by the symmetry conserved part, it increases to 45% for $n = 4$. As this contribution is negative, it stabilizes the solid

phase. Without it the theory strongly overestimates the stability of the fluid phase especially for softer potentials. This explains why the Ramakrishanan - Yussouff theory gives good results for hard core potentials but fails for potentials that have soft core and/or attractive tail.

The other point to be noted from these results is about the convergence of the series (2.29) which has been used to calculate $c^{(b)}(\vec{r}_1, \vec{r}_2)$. The contribution made by the second term of the series to the grand thermodynamic potential at the freezing point is found to be negligible compared to that of the first term for $n \geq 6$ and for $n < 6$, though the contribution is small but not negligible. For example, while for $n = 6$ this contribution is about 2% of the first term, for $n = 4$ this increases to 18%. From these results one can conclude that the first two terms of the series of Eq.(2.29) are enough to describe the freezing transition for a wide class of potentials.

In Table II, we compare results of freezing parameters γ_l , γ_s , $\Delta\gamma$, Lindemann parameter L_n and $\frac{P\sigma^3}{\epsilon}$ where P is the pressure at the transition point, of the present calculation with those found from computer simulations [21–28] and with the results found by others [12, 30–32] using approximate free energy functionals. The Lindemann parameter is defined as the ratio of the mean field displacement of a particle to the nearest neighbour distance in the crystal. For the fcc crystal with the Gaussian density profile of Eq.(3.13) it is given as

$$L_n = \left(\frac{3}{a_{fcc}^2 \alpha} \right)^{1/2}, \quad (4.1)$$

where $a_{fcc} = (4/\rho_0)^{1/3}$ is the fcc lattice constant. For the bcc crystal,

$$L_n = \left(\frac{2}{a_{bcc}^2 \alpha} \right)^{1/2}, \quad (4.2)$$

where $a_{bcc} = (2/\rho_0)^{1/3}$ is the bcc lattice constant.

In Fig. 12 we plot γ_l vs $1/n$ at the transition found from simulations and from the present calculations.

One may note that simulation results have spread (see Table II) and do not agree within each others uncertainties. This may be due to application of different theoretical methods used in locating the transition and system sizes in the calculations. The other sources of

errors include the existence of an interface, truncation of the potential, free-energy bias, etc. Agrawal and Kofke [25] who have reported results for $0 \leq 1/n \leq 0.33$ have considered a system of 500 particles only. Since they have not used finite size corrections, their results for softer potentials (say $n \lesssim 6$) may not be accurate. For example, they reported that for $1/n > 0.16$ fluid freezes into a bcc structure but for $1/n = 0.25$ they found that γ_l for the fluid - bcc transition is higher than that of the fluid-fcc transition. The recent calculations where large systems have been considered [26–28] results are available for $n \geq 5$ (or $1/n < 0.2$). From these results it is found that fluid freezes into fcc crystal for $n \geq 7$ and for $n < 7$ the bcc structure is preferred; the fluid-bcc-fcc triple point is estimated to be close to $1/n \sim 0.15$.

From Table II and Fig. 12 we find that our results are in very good agreement with simulation results for all cases. We find that for $n > 6.5$ the fluid freezes into fcc structure while for $n \leq 6$ it freezes into bcc structure. The fluid-bcc-fcc triple point is found at $\frac{1}{n} = 0.158$ (see the inset in Fig. 12). The value of Lindemann parameter found by us is, however, somewhat lower than those found by Agrawal and Kofke [25] and Saija et al [29]. The energy difference between the two cubic structures at the transition is found to be small in agreement with the simulation results [28].

V. SUMMARY AND PERSPECTIVES.

We used a free energy functional for a crystal proposed by Singh and Singh [13] to investigate the crystallization of fluids interacting via power law potentials. This free-energy functional was found by performing double functional integration in the density space of a relation that relates the second functional derivative of $A[\rho]$ with respect to $\rho(\vec{r})$ to the DPCF of the crystal. The expression found for $A[\rho]$ is exact and contains both the symmetry conserved part of the DPCF, $c^{(0)}(r, \rho)$ and the symmetry broken part $c^{(b)}(\vec{r}_1, \vec{r}_2)$. The symmetry conserved part corresponds to the isotropy and homogeneity of the phase and passes smoothly to the frozen phase at the freezing point, whereas the symmetry broken part arises due to heterogeneity which sets in at the freezing point and vanishes in the liquid phase. The values of $c^{(0)}(r)$ and its derivatives with respect to density ρ as a function of interparticle separation r have been determined using an integral equation theory comprising the OZ equation and the closer relation of Roger and Young [20]. From the results of $\frac{\partial c^{(0)}(r)}{\partial \rho}$

and $\frac{\partial^2 c^{(0)}(r)}{\partial \rho^2}$ we calculated the three- and four-bodies direct correlation functions of the isotropic phase. These results have been used in a series written in ascending powers of the order parameters to calculate $c^{(b)}(\vec{r}_1, \vec{r}_2)$. The contributions made by the first and second terms of the series have been calculated for bcc and fcc crystals. The contribution made by second term is found to be considerably smaller than the first term indicating that the first two terms are enough to give accurate values for $c^{(b)}(\vec{r}_1, \vec{r}_2)$. The values of $c^{(G)}(\vec{r})$ for bcc and fcc structures are found to differ considerably.

The contribution of symmetry broken part of DPCF to the free energy is found to depend on the nature of pair potentials; the contribution increases with softness of potentials. In case of power law potentials we found that the contribution to the grand thermodynamic potential at the freezing point arising from the second term of the series (2.29) which involves four-body direct correlation function is negligible for $n > 6$ and small but not negligible for $n < 6$. For $n = 4$ the contribution made by the second term is about 18% of the first term. The contribution made by second term is positive whereas the contribution of the first term is negative. As the net contribution made by the symmetry broken term is negative, it stabilizes the solid phase. Without the inclusion of this term the theory strongly overestimates the stability of the fluid phase especially for softer potentials. Our results reported in this paper and elsewhere [14, 17] explain why the Ramakrishanan - Yussouff theory gives good results for hard core potentials but fails for potentials that have soft core /or attractive tail.

The agreement between theory and simulation values of freezing parameters found for potentials with n varying from 4 to ∞ indicates that the free energy functional used here with values of $c^{(b)}(\vec{r}_1, \vec{r}_2)$ calculated from the first two terms of the series (2.29) provides an accurate theory for freezing transitions for a wide class of potentials. Since this free energy functional takes into account the spontaneous symmetry breaking, it can be used to study various phenomena of ordered phases near their melting points.

Acknowledgements: One of us (A.S.B.) thanks University Grants Commission (New Delhi, India) for award of research fellowship.

Appendix A

In this appendix we calculate $c_3^{(0)}(\vec{r}_1, \vec{r}_2, \vec{r}_3)$ and $c_4^{(0)}(\vec{r}_1, \vec{r}_2, \vec{r}_3, \vec{r}_4)$. Using the notation $r = |\vec{r}_2 - \vec{r}_1|$, $r' = |\vec{r}_3 - \vec{r}_1|$ and $|\vec{r}' - \vec{r}| = |\vec{r}_3 - \vec{r}_2|$ we write $c_3^{(0)}(\vec{r}_1, \vec{r}_2, \vec{r}_3)$ as (see Eq.(2.23))

$$c_3^{(0)}(\vec{r}, \vec{r}') = t(r)t(r')t(|\vec{r}' - \vec{r}|). \quad (\text{A1})$$

The function $t(|\vec{r}' - \vec{r}|)$ can be expanded in spherical harmonics,

$$t(|\vec{r}' - \vec{r}|) = \frac{2}{\pi} \sum_{lm} A_l(r, r') Y_{lm}(\hat{r}) Y_{lm}^*(\hat{r}'), \quad (\text{A2})$$

where,

$$A_l(r, r') = \int_0^\infty dq q^2 t(q) j_l(qr) j_l(qr'). \quad (\text{A3})$$

Here $j_l(x)$ is the spherical Bessel function and $Y_{lm}(\hat{r})$ the spherical harmonics.

From Eqs.(A1) and (A2) we get

$$c_3^{(0)}(\vec{r}, \vec{r}') = \frac{2}{\pi} \sum_{lm} D_l(r, r') Y_{lm}(\hat{r}) Y_{lm}^*(\hat{r}'), \quad (\text{A4})$$

where

$$D_l(r, r') = A_l(r, r') t(r) t(r').$$

The Fourier transform of Eq.(A4) defined as

$$\hat{c}_3^{(0)}(\vec{q}_1, \vec{q}_2) = \rho^2 \int d\vec{r} \int d\vec{r}' e^{-i\vec{q}_1 \cdot \vec{r}} e^{-i\vec{q}_2 \cdot \vec{r}'} c_3^{(0)}(\vec{r}, \vec{r}'),$$

gives

$$\hat{c}_3^{(0)}(\vec{q}_1, \vec{q}_2) = 32\pi \sum_{lm} (-1)^l D_l(q_1, q_2) Y_{lm}(\hat{q}_1) Y_{lm}^*(\hat{q}_2), \quad (\text{A5})$$

where,

$$D_l(q_1, q_2) = \rho^2 \int dr r^2 \int dr' r'^2 j_l(q_1 r) j_l(q_2 r') D_l(r, r'). \quad (\text{A6})$$

The value of $\hat{c}_3^{(0)}(\vec{q}_1, \vec{q}_2)$ is plotted in Fig. 13 for $q_1 = q_2 = q_{max}$ for various angle θ such that $0 < |\vec{q}_1 + \vec{q}_2| < 2q_{max}$, where θ is angle between \vec{q}_1 and \vec{q}_2 as shown in the figure. The values plotted in this figure correspond to $qa_0 = 4.3$ and for $n = 6$, $\gamma_l = 2.30$ (full line) and $n = 12$, $\gamma_l = 1.17$ (dashed line). In Fig. 14 we plot values of $\hat{c}_3^{(0)}(\vec{q}_1, \vec{q}_2)$ for equilateral triangle with various side lengths. The values for $n = 12$, $\gamma_l = 1.17$ are in good agreement with the values given in ref [6] (see Figs. 3 and 4 of ref [6]).

For $c_4^{(0)}(\vec{r}_1, \vec{r}_2, \vec{r}_3, \vec{r}_4)$ the contribution arises from three diagrams shown in Eq.(2.28). Using the notation $|\vec{r}_4 - \vec{r}_1| = r''$, $|\vec{r}_4 - \vec{r}_2| = |\vec{r}'' - \vec{r}|$, $|\vec{r}_4 - \vec{r}_3| = |\vec{r}'' - \vec{r}'|$ and other notations defined above we get

$$c_4^{(0)}(\vec{r}, \vec{r}', \vec{r}'') = \begin{array}{c} \begin{array}{ccc} \circ_4 & & \circ_3 \\ \vdots & \diagdown & \vdots \\ \circ_1 & & \circ_2 \end{array} + \begin{array}{ccc} \circ_4 & & \circ_3 \\ \vdots & \diagdown & \vdots \\ \circ_1 & & \circ_2 \end{array} + \begin{array}{ccc} \circ_3 & & \circ_4 \\ \vdots & \diagdown & \vdots \\ \circ_1 & & \circ_2 \end{array}, \end{array} \quad (\text{A7})$$

Each diagram of Eq.(A7) has two circles connected by three bonds- two s - bonds (dashed line) and one t - bond (full line), one of the remaining circles is connected by two t - bonds and the other by two s - bonds. By permuting circles one can convert one diagram into another. The values of $c_4^{(0)}(\vec{r}, \vec{r}', \vec{r}'')$ depend on three vectors \vec{r} , \vec{r}' and \vec{r}'' .

We calculate $\hat{c}_4^{(0)}(\vec{q}_1, \vec{q}_2, \vec{q}_3)$ defined as

$$\hat{c}_4^{(0)}(\vec{q}_1, \vec{q}_2, \vec{q}_3) = \rho^3 \int d\vec{r} \int d\vec{r}' \int d\vec{r}'' e^{-i\vec{q}_1 \cdot \vec{r}} e^{-i\vec{q}_2 \cdot \vec{r}'} e^{-i\vec{q}_3 \cdot \vec{r}''} c_4^{(0)}(\vec{r}, \vec{r}', \vec{r}''), \quad (\text{A8})$$

Using Eq.(A7) and writing each diagram in terms of t and s bonds we get

$$\begin{aligned} \hat{c}_4^{(0)}(\vec{q}_1, \vec{q}_2, \vec{q}_3) &= \frac{108}{\pi^2} \sum_{l_1 m_1} \sum_{l_2 m_2} \sum_{l_3 m_3} (-i)^{(l_1 + l_2 + l_3)} \Lambda_{l_1 l_2 l_3}^{m_1 m_2 m_3} M_{l_1 l_2 l_3}(q_1, q_2, q_3) \\ &\quad [Y_{l_3 m_3}^*(\hat{q}_1) Y_{l_1 m_1}(\hat{q}_2) Y_{l_2 m_2}(\hat{q}_3) + Y_{l_1 m_1}(\hat{q}_1) Y_{l_3 m_3}^*(\hat{q}_2) Y_{l_2 m_2}(\hat{q}_3) \\ &\quad + (-1)^{l_1} Y_{l_1 m_1}(\hat{q}_1) Y_{l_3 m_3}^*(\hat{q}_2) Y_{l_2 m_2}(\hat{q}_3)], \end{aligned} \quad (\text{A9})$$

where

$$\Lambda_{l_1 l_2 l_3}^{m_1 m_2 m_3} = \left[\frac{(2l_1 + 1)(2l_2 + 1)}{4\pi(2l_3 + 1)} \right]^{1/2} C_g(l_1, l_2, l_3; 0, 0, 0) C_g(l_1, l_2, l_3; m_1, m_2, m_3), \quad (\text{A10})$$

and

$$M_{l_1 l_2 l_3}(q_1, q_2, q_3) = \rho^3 \int_0^\infty dr r^2 s(r) \int_0^\infty d\vec{r}' r'^2 t(r') \int_0^\infty d\vec{r}'' r''^2 s(r'') \\ j_{l_3}(q_1 r) j_{l_1}(q_2 r') j_{l_2}(q_3 r'') A_{l_1}(r, r') E_{l_2}(r, r''). \quad (\text{A11})$$

$A_{l_1}(r, r')$ is defined by Eq.(A3). $E_{l_2}(r, r'')$ is given as

$$E_l(r, r'') = \int_0^\infty dq q^2 s(q) j_l(qr) j_l(qr''). \quad (\text{A12})$$

The values of $\hat{c}_4^{(0)}(\vec{q}_1, \vec{q}_2, \vec{q}_3)$ depend on magnitudes and directions of vectors \vec{q}_1 , \vec{q}_2 and \vec{q}_3 . In Figs. 15 and 16 we use color codes (shown at the right hand side of each figure) to plot values of $\hat{c}_4^{(0)}(\vec{q}_1, \vec{q}_2, \vec{q}_3)$ for $q_1 = q_2 = q_3 = q_{max}$ as a function of ϕ_{q_2} and ϕ_{q_3} for different choices of θ_{q_2} and θ_{q_3} . The values of $q_{max} a_0$ is taken equal to 4.3 as in Fig. 13. While the values plotted in Fig. 15 correspond to $\theta_{q_1} = 0^\circ$, the values plotted in Fig. 16 correspond to $\theta_{q_1} = 90^\circ$ and $\phi_{q_1} = 0^\circ$. These figures show how the values of $\hat{c}_4^{(0)}(\vec{q}_1, \vec{q}_2, \vec{q}_3)$ depend on orientations of vectors \vec{q}_1 , \vec{q}_2 and \vec{q}_3 . Emergence of ordering in maxima and minima depending on orientations of these vectors is evident.

-
- [1] J. G. Kirkwood and E. Monroc, J. Chem. Phys. **9**, 514 (1951).
 - [2] Y. Singh, Phys. Rep. **207**, 351 (1991).
 - [3] H. Lowen, Phys. Rep. **237**, 249(1994).
 - [4] T. V. Ramakrishnan and M. Yussouff, Phys. Rev. B **19**, 2775 (1979).
 - [5] A. D. J. Haymet and D. W. Oxtoby, J. Chem. Phys. **74**, 2559 (1981).
 - [6] J. L. Barrat, J. P. Hansen and G. Pastore, Mol. Phys. **63**, 747 (1988); Phys. Rev. Lett. **58**, 2075(1987).
 - [7] W. A. Curtin, J. Chem. Phys. **88**, 7050 (1988).
 - [8] P. Tarazona, Phys. Rev. A **31**, 2672 (1985).

- [9] W. A. Curtin and N. W. Ashcroft, Phys. Rev. A **32**, 2909 (1985).
- [10] A. R. Denton and N. W. Ashcroft, Phys. Rev. A **39**, 4701 (1989).
- [11] C. N. Likos and N. W. Ashcroft, J. Chem. Phys. **99**, 9090 (1993).
- [12] D. C. Wang and A. P. Gast, J. Chem. Phys. **110**, 2522(1999).
- [13] S. L. Singh and Y. Singh, Europhys. Lett. **88**, 16005 (2009)
- [14] S. L. Singh, A. S. Bharadwaj and Y. Singh, Phys. Rev. E **83**, 051506 (2011)
- [15] J. P. Hansen and I. R. McDonald, **Theory of Simple Liquids, 3rd ed** (Academic press, Boston, 2006)
- [16] P. Mishra and Y. Singh, Phys. Rev. Lett. **97**, 177801 (2006);
P. Mishra, S. L. Singh, J. Ram and Y. Singh, J. Chem. Phys. **127**, 044905 (2007).
- [17] A. Jaiswal, S. L. Singh and Y. Singh, Phys. Rev. E **87**, 012309 (2013).
- [18] J. S. McCarley and N. W. Ashcroft, Phys. Rev. E **55**, 4990 (1997).
- [19] A. Jaiswal and Y. Singh, unpublished.
- [20] F. J. Rogers and D. A. Young, Phys. Rev. A **30**,999, (1984).
- [21] W. G. Hoover, M. Ross, K. W. Johnson, D. Henderson, J. A. Barker, and B. C. Brown, J. Chem. Phys. **52**, 4931 (1970).
- [22] W. G. Hoover and F. H. Ree, J. Chem. Phys. **49**, 3609 (1968)
- [23] B. J. Alder, W. G. Hoover and D. A. Young, J. Chem. Phys. **49**, 3688 (1968).
- [24] H. Ogura, H. Matsuda, T. Ogawa, N. Ogita, and A. Veda, Prog. Theor. Phys. **58**, 419 (1992).
- [25] R. Agrawal and D.A. Kofke, Mol. Phys. **85**, 23 (1995).
- [26] R.L. Davidchack and B.B. Laird, Phys. Rev. Lett. **94**, 086102 (2005).
- [27] T. B. Tan, A. J. Schultz and D. A. Kofke, Mol. Phys. **109**, 123 (2011).
- [28] S. Prestipino, F. Saija, and P. V. Giaquinta, J. Chem. Phys. **123**, 144110 (2005).
- [29] F. Saija, S. Prestipino, and P. V. Giaquinta, J. Chem. Phys. **124**, 244504 (2006).
- [30] J. L. Barrat, J. P. Hansen and G. Pastore and E. M. Waisman, J. Chem. Phys. **86**, 6360(1987).
- [31] B. B. Laird, J. D. McCoy and A. D. J. Heymat, J. Chem. Phys. **87**, 5449 (1987).
- [32] B. B. Laird, and D. M. Kroll, Phys. Rev. A. **42**, 4810 (1990).

TABLE I: Freezing parameters γ_l , $\Delta\gamma$ and the contributions of ideal symmetry conserving and symmetry broken parts arising from first and second terms of Eq.(2.29) to $\Delta W/N$ at the transition point.

n	<i>Lattice</i>	γ_l	$\Delta\gamma$	$\Delta W_{id}/N$	$\Delta W_o/N$	$\Delta W_b^{(1)}/N$	$\Delta W_b^{(2)}/N$
4	bcc	5.57	0.007	2.86	-2.09	-0.94	0.17
	fcc	5.60	0.008	3.52	-2.64	-1.03	0.15
6	bcc	2.30	0.011	2.56	-1.99	-0.58	0.01
	fcc	2.32	0.012	3.48	-2.75	-0.72	0.002
6.5	bcc	2.04	0.014	2.38	-1.89	-0.50	0.001
	fcc	2.03	0.013	3.34	-2.69	-0.66	0.001
7	bcc	1.86	0.015	2.29	-1.85	-0.44	0.000
	fcc	1.84	0.014	3.39	-2.76	-0.63	0.000
12	fcc	1.17	0.034	3.71	-3.14	-0.57	0.000
∞	fcc	0.937	0.106	4.44	-4.10	-0.34	0.000

TABLE II: Comparison of parameters γ_l , γ_s , $\Delta\gamma$, the Lindemann parameter L and the pressure P at the coexistence found from different free-energy functional and computer simulations. MWDA stands for modified weighted density approximation, RY DFT stands for Ramakrishnan - Yussouff Density functional theory. MHNC stands for modified hypernetted-chain closure relation and MSMC for Mayer sampling Monte Carlo.

n	<i>Lattice</i>	Theory/ Simulation	γ_l	γ_s	$\Delta\gamma$	L	$\frac{P\sigma^3}{\epsilon}$
∞	fcc	Present result	0.937	1.036	0.106	0.09	11.46
		MWDA-static reference [12]	0.863	0.964	0.115	0.13	
		MWDA [32]	0.906	1.044	0.116	0.10	
		RY DFT [30, 31]	0.980	1.146	0.174	0.06	
		Simulation [22]	0.939	1.037	0.104	~ 0.13	
		Simulation [23]	0.942	1.041	0.105		
		MC Simulation [25]	0.94	1.041	0.107	0.12	

Continued on next page

TABLE II – *Continued from previous page*

n	Lattice	Theory/ Simulation	γ_l	γ_s	$\Delta\gamma$	L	$\frac{P\sigma^3}{\epsilon}$
		MC Simulation [26]	0.939	1.037	0.104		11.57
12	fcc	Present result	1.17	1.21	0.034	0.11	23.67
		MWDA-static reference [12]	1.12	1.16	0.037	0.14	
		MWDA/MHNC [32]	1.19	1.26	0.059	0.10	
		MC Simulation* [25]	1.17	1.22	0.042	0.14	23.64
		MSMC technique [27]	1.16	1.20	0.037		23.24
		MC Simulation [26]	1.16	1.21	0.037		23.41
7	fcc	Present result	1.84	1.87	0.014	0.12	64.97
		MC Simulation* [25]	1.85	1.88	0.017	0.15	64.98
		MC Simulation [26]	1.84	1.87	0.016		64.22
	bcc	Present result	1.86	1.89	0.015	0.18	67.12
		MC Simulation [26]	1.83	1.86	0.015		63.88
6.5	fcc	Present result	2.03	2.06	0.013	0.12	80.11
		MC Simulation* [25]	2.04	2.07	0.014	0.15	80.40
	bcc	Present result	2.04	2.07	0.014	0.17	78.98
		MC Simulation* [28, 29]	2.03	2.05	0.010	0.18	78.40
6	fcc	Present result	2.32	2.35	0.012	0.12	103.7
		MWDA-static reference [12]	2.33	2.35	0.007	0.17	
		MC Simulation* [25]	2.34	2.37	0.012	0.15	104.5
		MC Simulation [26]	2.32	2.35	0.012		103.0
	bcc	Present result	2.30	2.33	0.011	0.16	101.22
		MC Simulation* [25]	2.32	2.35	0.011	0.17	103.6
		MSMC technique [27]	2.30	2.32	0.011		100.1
		MC Simulation [26]	2.30	2.33	0.012		100.0
		MC Simulation* [28, 29]	2.29	2.31	0.009	0.18	99.34
4	fcc	Present result	5.60	5.63	0.008	0.12	565.6
		MWDA-static reference [12]	5.22	5.26	0.008	0.13	
		MC Simulation [25]	5.68	5.71	0.005	0.17	637.0
	bcc	Present result	5.57	5.61	0.007	0.16	561.2
		MWDA-static reference [12]	5.05	5.09	0.008	0.18	
		MC Simulation [25]	5.73	5.75	0.004	0.18	648.0

NOTE-* indicates values obtained from interpolation of the tabulated values.

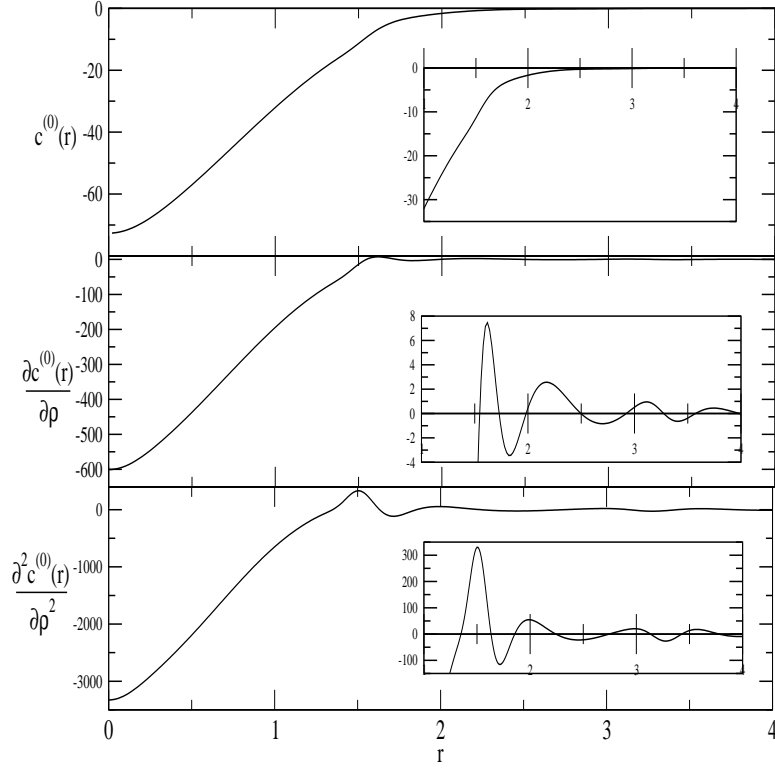


FIG. 1: Plots of $c^{(0)}(r)$, $\frac{\partial c^{(0)}(r)}{\partial \rho}$ and $\frac{\partial^2 c^{(0)}(r)}{\partial \rho^2}$ vs r for $n = 6$ and $\gamma = 2.30$ which is close to the freezing point. The distance r is in unit of $a_0 = \left(\frac{3}{4\pi\rho}\right)^{1/3}$. Insets show magnified values of respective quantities for $r \geq 1$.

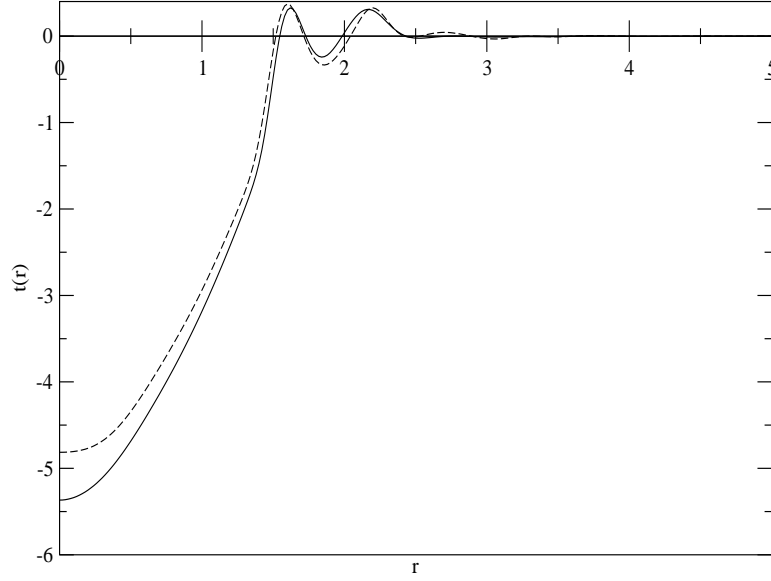


FIG. 2: Plot of $t(r)$ vs r for $n = 6$ at $\gamma = 2.32$ and $n = 4$ at $\gamma = 5.60$. The distance r is in unit of $a_0 = \left(\frac{3}{4\pi\rho}\right)^{1/3}$. The dashed curve represents values for $n = 4$, $\gamma_l = 5.60$ and full curve for $n = 6$, $\gamma_l = 2.32$.

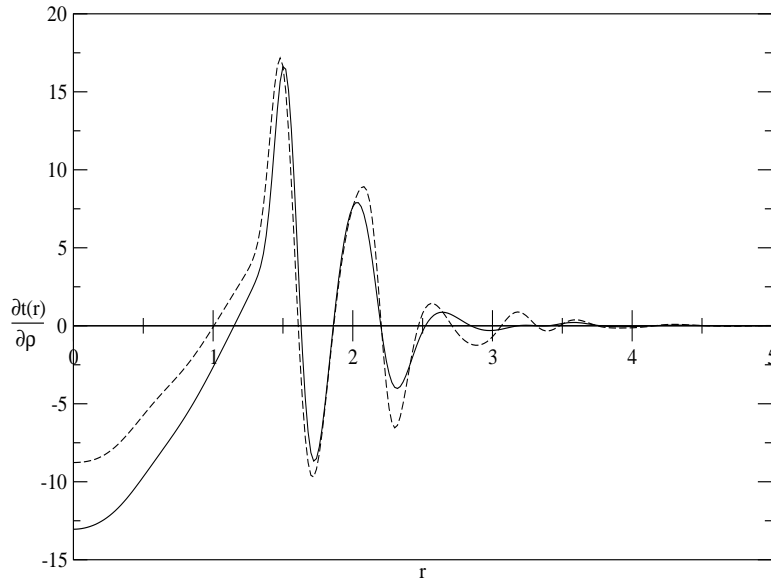


FIG. 3: Plot of $\frac{\partial t(r)}{\partial \rho}$ vs r for $n = 6$ at $\gamma = 2.32$ and $n = 4$ at $\gamma = 5.60$. Other notations are same as in Fig. 2.

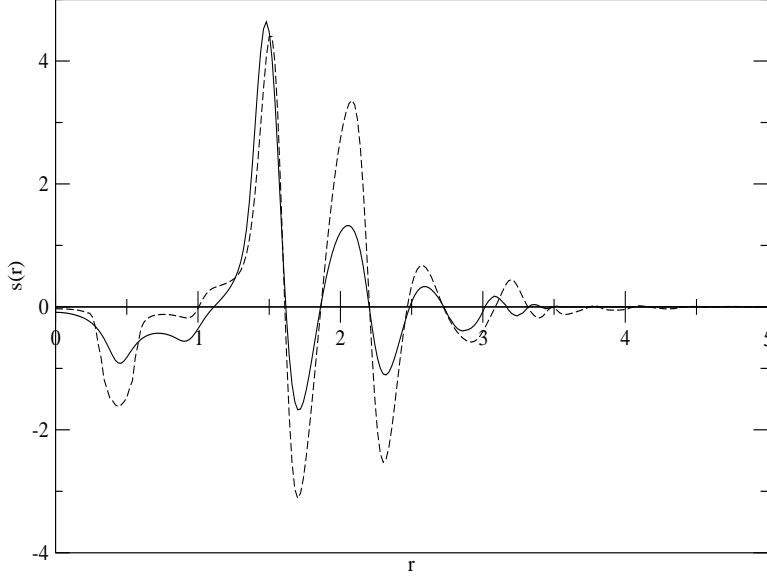


FIG. 4: Plot of $s(r)$ vs r for $n = 6$ at $\gamma = 2.32$ and $n = 4$ at $\gamma = 5.60$. Other notations are same as in Fig. 2.

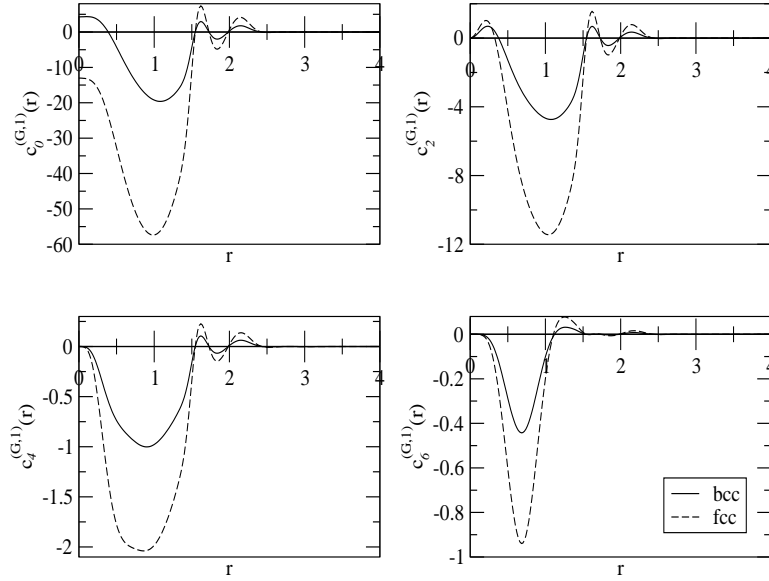


FIG. 5: Comparison of values of $c_i^{(G,1)}(r)$ as a function of r for a G vector of first set of fcc and bcc lattices for $n = 6$, $\gamma_s = 2.32$, $\alpha_{fcc} = 32$ and $\alpha_{bcc} = 18$. The distance r is in unit of $a_0 = \left(\frac{3}{4\pi\rho}\right)^{1/3}$ and $\mu = e^{-G^2/4\alpha}$. The dashed curve represents values of fcc structure while full curve of bcc structure.

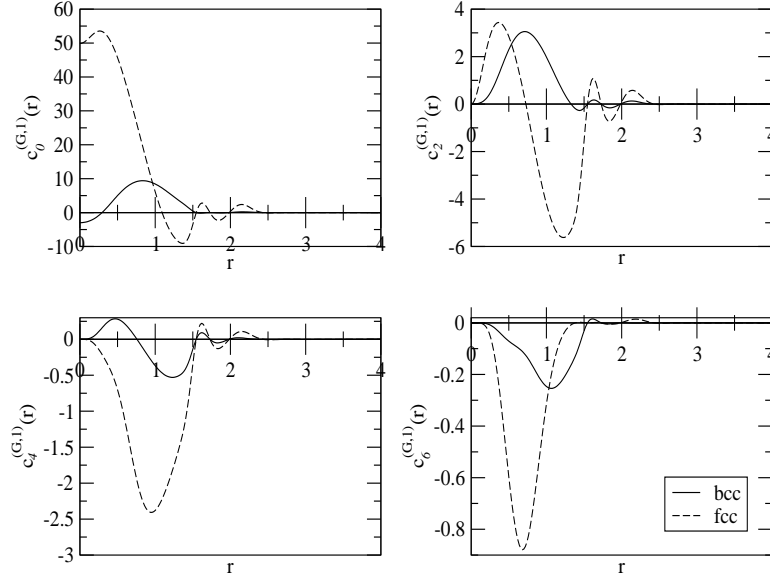


FIG. 6: Comparison of values of $c_l^{(G,1)}(r)$ as a function of r for a G vector of second set of fcc (dashed curve) and bcc (full curve) lattices for $n = 6$, $\gamma_s = 2.32$, $\alpha_{fcc} = 32$ and $\alpha_{bcc} = 18$. Other notations are same as in Fig. 5.

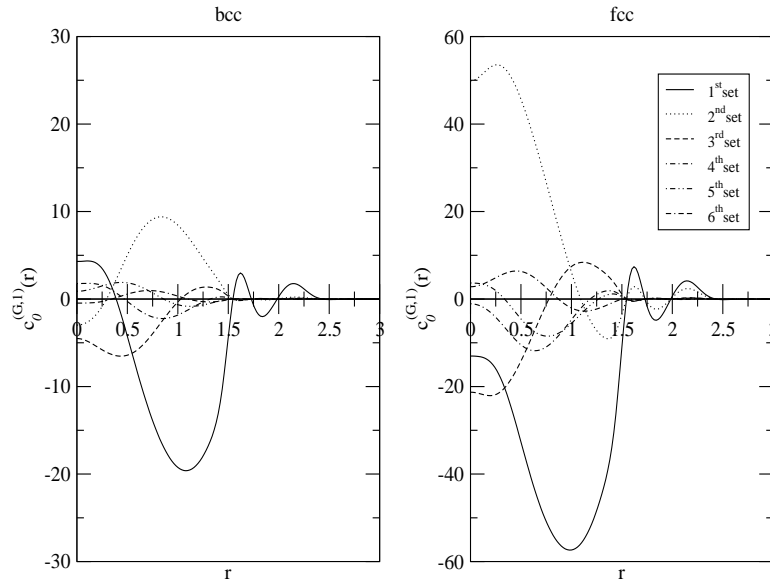


FIG. 7: Comparison of values of $c_0^{(G,1)}(r)$ as a function of r for a G vector of the first six sets of fcc and bcc lattices. The distance r is in unit of $a_0 = \left(\frac{3}{4\pi\rho}\right)^{1/3}$.

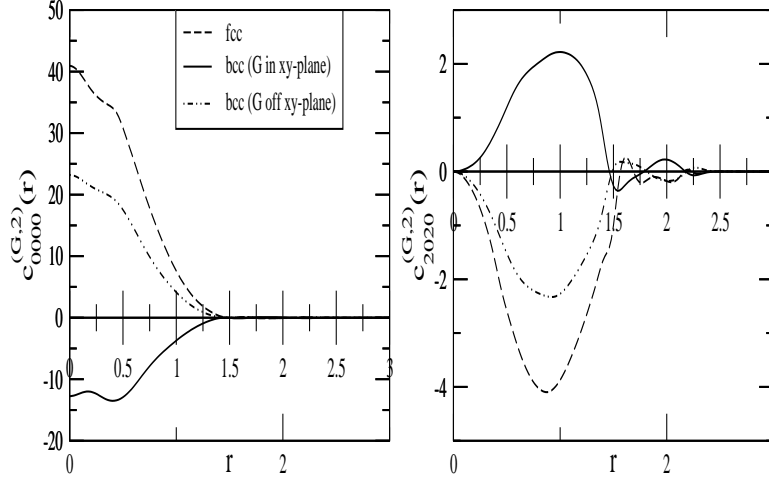


FIG. 8: Comparison of values of $c_{lml'm'}^{(G,2)}(r)$ as a function of r for a G vector of the first set of fcc and bcc lattices for $n = 6$ at $\gamma_s = 2.32$, $\alpha_{fcc} = 32$ and $\alpha_{bcc} = 18$. The distance r is in unit of $a_0 = \left(\frac{3}{4\pi\rho}\right)^{1/3}$. There is two sets of values for bcc lattice; one for \vec{G} vectors lying in x-y plane and the other for the rest of \vec{G} vectors of the first set. There is only one set of values for fcc lattice.

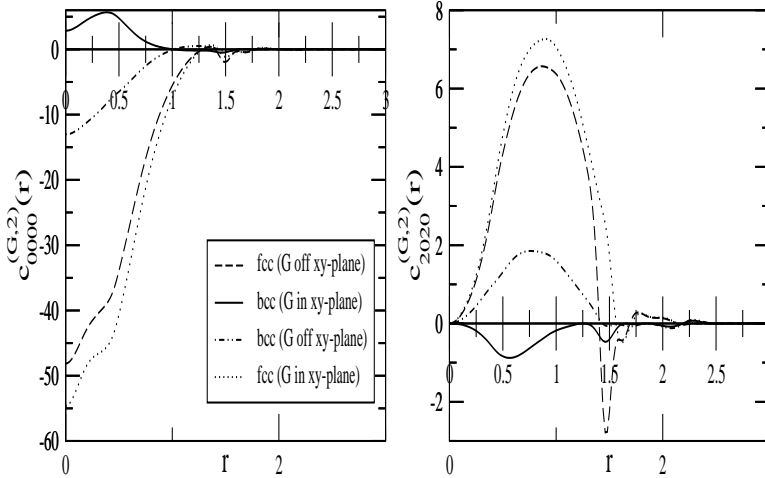


FIG. 9: Comparison of values of $c_{lml'm'}^{(G,2)}(r)$ as a function of r for a G vector of the second set of fcc and bcc lattices. Other notations are same as in Fig. 8, except that there is now two sets of values shown by dashed and dotted curves for fcc lattice (see text)

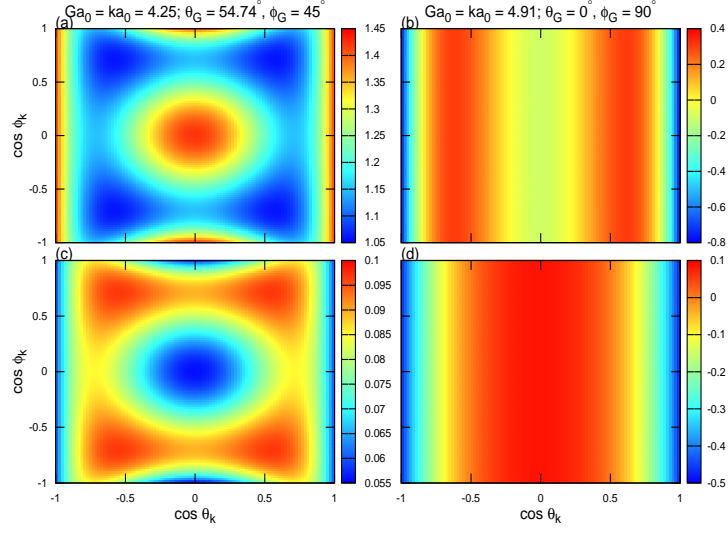


FIG. 10: Comparison of values (shown using color codes given on right hand side of each figure) of $c^{(G,1)}(k, \theta_k, \phi_k)$ and $c^{(G,2)}(k, \theta_k, \phi_k)$ as a function of $\cos\theta_k$ (plotted on x-axis) and $\cos\phi_k$ (plotted on y-axis) for $G_1 a_0 = ka_0 = 4.25$, $\theta_{G_1} = 54.7^\circ$, $\phi_{G_1} = 45^\circ$ (a and c) and $G_2 a_0 = ka_0 = 4.91$, $\theta_{G_2} = 0^\circ$, $\phi_{G_2} = 90^\circ$ (b and d) for a fcc lattice for $n = 6$, $\gamma_s = 2.32$, $\alpha_{fcc} = 32$.

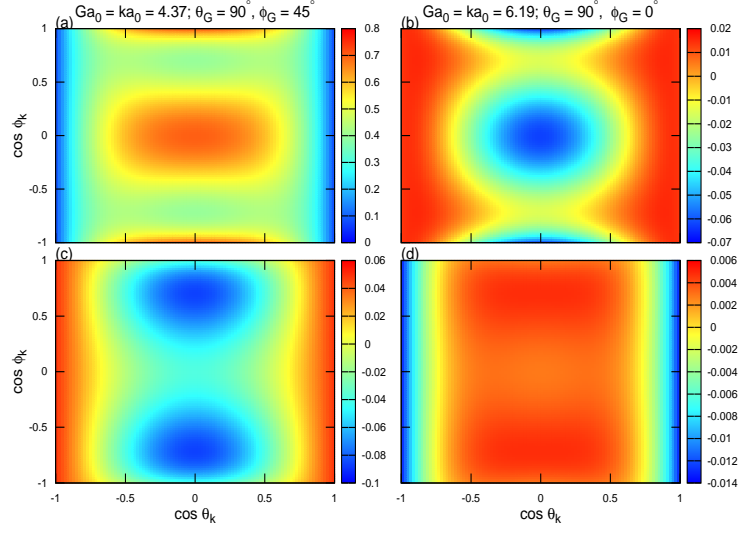


FIG. 11: Comparison of values (given in a color code) of $c^{(G,1)}(k, \theta_k, \phi_k)$ and $c^{(G,2)}(k, \theta_k, \phi_k)$ as a function of $\cos \theta_k$ and $\cos \phi_k$ for $G_1 a_0 = ka_0 = 4.37$, $\theta_{G_1} = 90^\circ$, $\phi_{G_1} = 45^\circ$ (a and c) and $G_2 a_0 = ka_0 = 6.19$, $\theta_{G_2} = 90^\circ$, $\phi_{G_2} = 0^\circ$ (b and d) for a bcc lattice for $n = 6$, $\gamma_s = 2.32$, $\alpha_{bcc} = 18$. Other notation are same as in Fig. 10

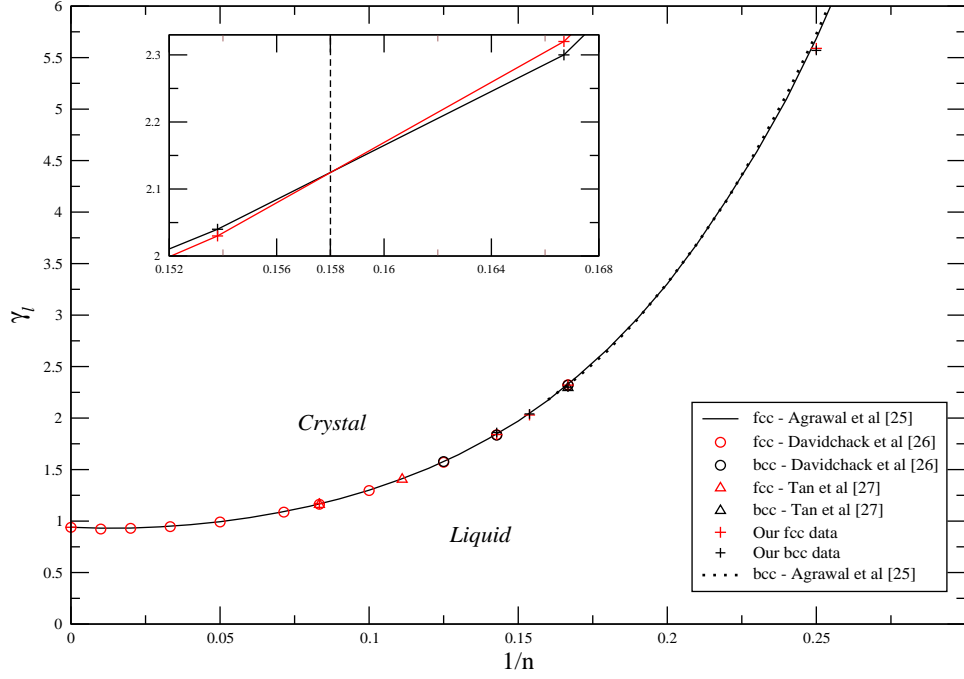


FIG. 12: Comparison of equilibrium phase diagram of $\frac{1}{n}$ vs γ_l found from simulation results and from our theory. In inset the fluid-fcc and fluid-bcc transition lines are plotted at a magnified scale and the fluid-bcc-fcc triple point is found at $\frac{1}{n} = 0.158$.

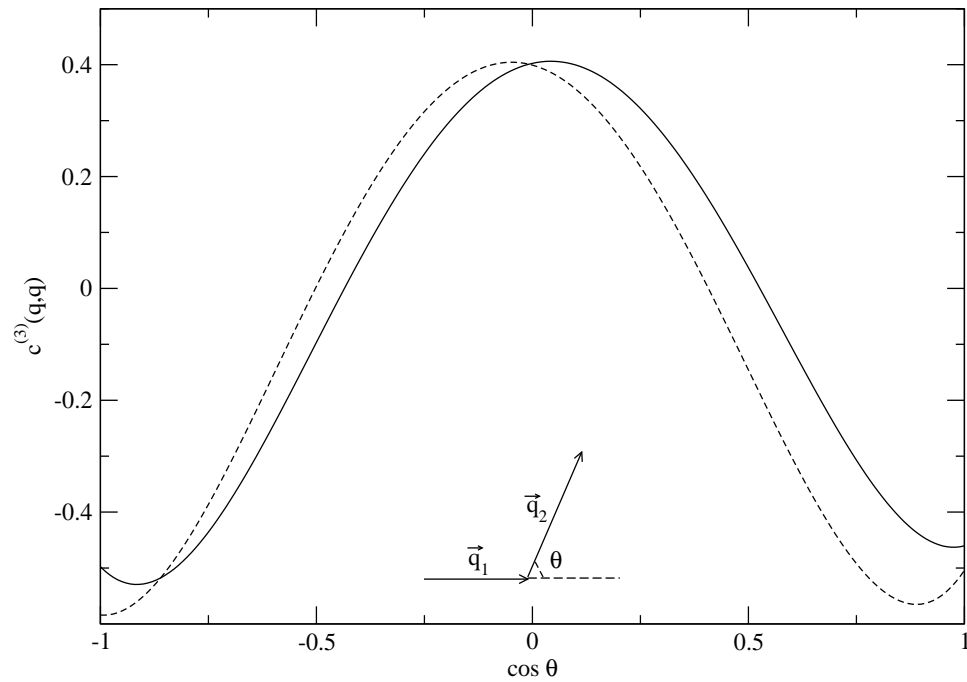


FIG. 13: Values of $\hat{c}_3^{(0)}(q, q, q)$ as a function of $\cos\theta$ (geometry is shown schematically in the figure) for $q_1 a_0 = q_2 a_0 = 4.3$ and for potentials $n = 12, \gamma_l = 1.17$ (dashed curve) and $n = 6, \gamma_l = 2.30$ (full curve)

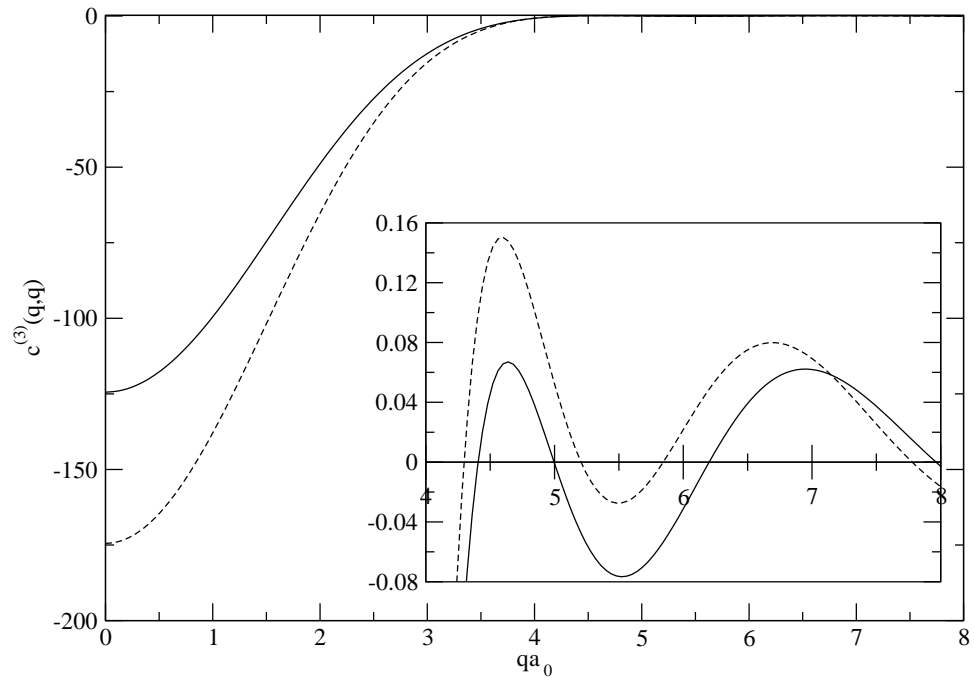


FIG. 14: Values of $\hat{c}_3^{(0)}(q, q, q)$ vs qa_0 (equilateral triangles). The dashed curve represents the values for $n = 12, \gamma_l = 1.17$ and full curve for $n = 6, \gamma_l = 2.30$. Inset shows values for $qa_0 \geq 4.0$ on magnified scale.

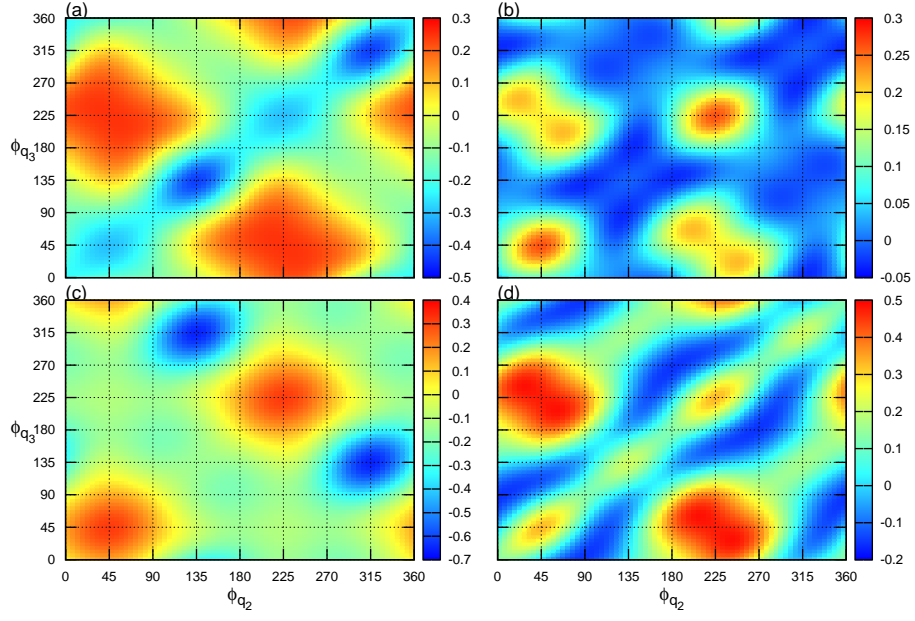


FIG. 15: Values of $\hat{c}_4^{(0)}(\vec{q}_1, \vec{q}_2, \vec{q}_3)$ (shown using a color code shown on right hand side of each figure) as a function of ϕ_{q_2} and ϕ_{q_3} for $q_1 = q_2 = q_{max}$ with $q_{max}a_0 = 4.3$, $\theta_{q_1} = 0^\circ$, $\phi_{q_1} = 0^\circ$: In (a) $\theta_{q_2} = 45^\circ$, $\theta_{q_3} = 45^\circ$, (b) $\theta_{q_2} = 45^\circ$, $\theta_{q_3} = 90^\circ$, (c) $\theta_{q_2} = 90^\circ$, $\theta_{q_3} = 45^\circ$, and (d) $\theta_{q_2} = 90^\circ$, $\theta_{q_3} = 90^\circ$

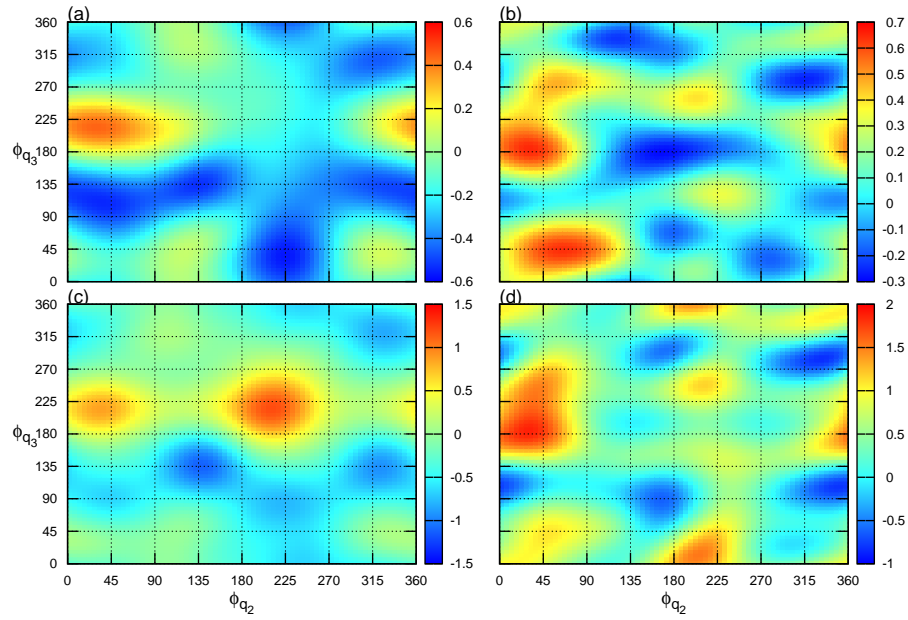


FIG. 16: Same as in Fig. 15 except $\theta_{q_1} = 90^\circ$ and $\phi_{q_1} = 0^\circ$